Supporting Information

2D $MoO_{3-x}S_x/MoS_2$ van der Waals Assembly: a Tunable Heterojunction with Attractive Properties for Photocatalysis

Masoud Shahrokhi [1], Pascal Raybaud [1,2*] and Tangui Le Bahers [1*]

[1] *Univ Lyon, ENS de Lyon, CNRS, Université Claude Bernard Lyon 1, Laboratoire de Chimie UMR 5182, F-69342 Lyon,France*

[2] *IFP Energies nouvelles, Rond-point de l'échangeur de Solaize, BP 3, 69360 Solaize, France*

Authors for correspondence: pascal.raybaud@ifpen.fr; tangui.le_bahers@ens-lyon.fr

Contents

S1. Methodology and Computational Setup

S1.1. Total energy calculations and electronic properties

Total energy calculations including geometry optimizations of all pristine and substituted single- and multi-layer structures were performed by the *ab initio* CRYSTAL17 code which works within periodic boundary conditions and adopts localized Gaussian-type function basis sets (BSs). The following BSs were used: Mo_SC_HAYWSC-311G(d31)_cora_1997[1] (for Mo atoms), S_86-311G*_lichanot_1993[2] (for S atoms) and O_8-411d11G_valenzano_2006[3] (for O atoms). For the exchange-correlation potential, the PBE functional[4] have been adopted and the van der Waals contributions were described by using the semi-empirical Grimme D3 approach[5] with optimized scaling factors[6]. The tolerances for the evaluation of Coulomb and exchange series are set to $8 \times 8 \times 8 \times 8 \times 16$.[7] Since ordinary DFT within the PBE/GGA underestimate the band gap, all the electronic properties were computed via single-point calculations by using the range separated hybrid Heyd–Scuseria–Ernzerhof (HSE06) exchange correlation functional[8] on the PBE optimized geometries using CRYSTAL17. All calculations (including geometry optimizations and electronic properties) were performed with an energy threshold of 10^{-10} Ha per unit-cell for the self-consistent field (SCF) process. The reciprocal space for the unit-cell of pristine 2D MoS_2 and MoO_3 systems is sampled according to a sublattice with a 12×12 k-point mesh. The k-point mesh sampling is progressively reduced as the size of the monolayer and multilayer unit cells increases for the doped materials (see Tables S3 and S4).

Three different energetic stability analysis were performed to analyze the stability of 2D $MoO_{3-x}S_x$ and $MoS_{2-x}O_x$ systems: (i) binding energy, (ii) reaction energy and (iii) thermodynamic phase diagram which were described in our previous work of the same systems in the bulk phase.[6]

S1.2. Optical properties

The optical properties in this work were calculated through the frequency dependent dielectric matrix $\varepsilon_{\alpha\beta}(\omega)$ within the HSE06 functional by using the Vienna *ab initio* simulation package (VASP).[9–11] The previously PBE optimized structures with CRYSTAL were used for the optical calculations. Electronic wave functions have been expanded using a plane wave basis set with a cutoff energy of 500 eV for the valence electrons and the interaction between the valence and the core electrons for Mo, O and S atoms was described with the projected augmented wave (PAW) method.[12] In all optical calculations a cell with a vacuum region of 20 Å in the direction normal to the sheet plane has been used to avoid image-image interactions. The number of empty conduction bands was converged for each structure with respect to standard calculations. The absorption coefficient can be evaluated from dielectric matrix using the Kramers-Kronig transformation:[13]

$$\alpha_{\alpha\beta}(\omega) = \frac{2\omega k_{\alpha\beta}(\omega)}{c} = \frac{\omega \mathrm{Im}(\varepsilon_{\alpha\beta}(\omega))}{c n_{\alpha\beta}(\omega)} \qquad (1)$$

where c is the speed of light in vacuum. $n_{\alpha\beta}$ and $k_{\alpha\beta}$ are real and imaginary parts of the complex refractive index, and are known as the refractive index and the extinction index, respectively. They are given by the following relations:

$$n_{\alpha\beta}(\omega) = \sqrt{\frac{|\varepsilon_{\alpha\beta}(\omega)| + \mathrm{Re}(\varepsilon_{\alpha\beta}(\omega))}{2}} \qquad (2) \qquad k_{\alpha\beta}(\omega) = \sqrt{\frac{|\varepsilon_{\alpha\beta}(\omega)| - \mathrm{Re}(\varepsilon_{\alpha\beta}(\omega))}{2}} \qquad (3)$$

S1.3. High frequency dielectric constant profile $\varepsilon_\infty(z)$

To obtain the local (microscopic) dielectric constant profiles, we followed a DFT scheme based on polarization variation in response to a finite electric field as recently proposed[14–16] to extract dielectric profiles in heterostructures. This method avoids the complete determination of the dielectric matrix, thus reducing the computational time.

In order to extract the optical (high frequency) dielectric constant profile along the out-of-plane direction (z-axis) in 2D systems, the calculated DFT electron density are analyzed in four steps. In the first step, the calculated electronic density with ($\rho(z)|\vec{E}_{ext}$) and without ($\rho(\rho(z)|_0$) external electric field using CRYSTAL package is averaged in the plane parallel to the z-axis. It is then smoothed using a nanoscale averaging[17] along the out-of-plane direction. It is noteworthy that for the high frequency limit (optical dielectric constant) only the electrons are considered to respond to the applied electric field whereas for lower frequencies (static dielectric constant) both electronic and ionic (phonons) effects are considered. In the second step, the induced electron density, $\delta\rho_{ind}(z)$, is computed by subtracting the results of electronic density with and without external electric field:

$$\delta\rho_{ind}(z) = \rho(z)|\vec{E}_{ext} - \rho(z)|_0 \quad (4)$$

The third step is computing the induced polarization, p_{ind} (z), by the partial integration of the induced electronic density:

$$\frac{dp_{ind}(z)}{dz} = -\delta\rho(z) \quad (5)$$

In the fourth step, the nanoscopic average of the high frequency dielectric constant profile $\varepsilon_\infty(z)$ is calculated from the induced polarization:

$$\varepsilon_\infty(z) = \frac{\varepsilon_0 E_{ext}}{\varepsilon_0 E_{ext} - p_{ind}(z)} \quad (6)$$

We can finally define the inverse of effective dielectric constant (ε_{eff}) of a 2D system (of height x_1-x_2) as the average of the inverse of local dielectric function:[18]

$$\frac{1}{\varepsilon_{eff}} = \frac{1}{x_2 - x_1}\int_{x_1}^{x_2} \frac{1}{\varepsilon_\infty(x)} dx \quad (7)$$

This method has been performed[15,16,19–21] to calculate dielectric constant profile using the local orbital SIESTA[22] code so far. For the first time we performed this method using the CRYSTAL results of electronic density. It is worth to note that the calculations presented in all previous published papers were performed using the simple LDA[23] or GGA[4] functional while in our current work we employed hybrid functional of HSE06[8] to provide more accurate estimations.

S2. Pristine structures of single- and few-layers MoO_3 and MoS_2

S2.1. Structures, binding energy and exfoliation energy

In order to model the MoO_3 and MoS_2 nanosheet structures, the primitive cell of 2D layers was directly cut from the optimized 3D α-MoO_3 and 2H-MoS_2 bulk structures along the direction of the vdW interaction. The crystal structures of single-layer (SL) and few-layer (FL) MoO_3 and MoS_2 systems is depicted in Figure S1a and b. In each layer of MoO_3 system, the orthorhombic lattice consists of 2 Mo and 6 O atoms where Mo atoms are an octahedral environment connected by covalent bonds to 1 O-oxo species and 5 bridging O atoms. The atomic arrangement in each layer of MoS_2 system (Figure S1b) is hexagonal, in which each Mo atom is surrounded at equal distances by 6 S atoms placed at the corners of a trigonal prism.

To evaluate the stability of pristine single- and few-layer MoO_3 structures, the binding energies (E_b) per MoO_3 were computed as

$$E_b = \left(\frac{E_{tot} - (n_{Mo}E_{Mo} + (\frac{1}{2})n_O E_{O_2})}{N}\right) \times 4 \quad (8)$$

and the binding energies of pristine single- and few-layer MoS_2 structures per MoS_2 were computed as

$$E_b = \left(\frac{E_{tot} - (n_{Mo}E_{Mo} + n_S E_{S\alpha}}{N}\right) \times 3 \quad (9)$$

where E_{tot} is the total energy per cell, E_i is the energy of the i-th individual elements in their respective ground states, n_i is the number of species i in the structure and N is the total number of atoms per cell.

The n-layer exfoliation energy per unit area $E_{exf}\,(n)$ is given by[24]

$$E_{exf}(n) = \frac{E_{iso}(n) - E_{bulk}\,n/m}{\mathcal{A}} \qquad (10)$$

where $E_{iso}\,(n)$ is the energy of the unit cell of an isolated n-layer slab in vacuum, E_{bulk} is the energy of the unit cell of a bulk material composed of m layers, thus E_{bulk}/m corresponds to the energy of the bulk per layer, and $\mathcal{A}$ is the in-plane area of the bulk unit cell.

According to our results, the lattice parameters and exfoliation energies of both MoO_3 and MoS_2 systems slightly increases as the number of layers is increased from monolayer to bulk, while the binding energy is decreased (see Figure S1, Tables S1 and S2).

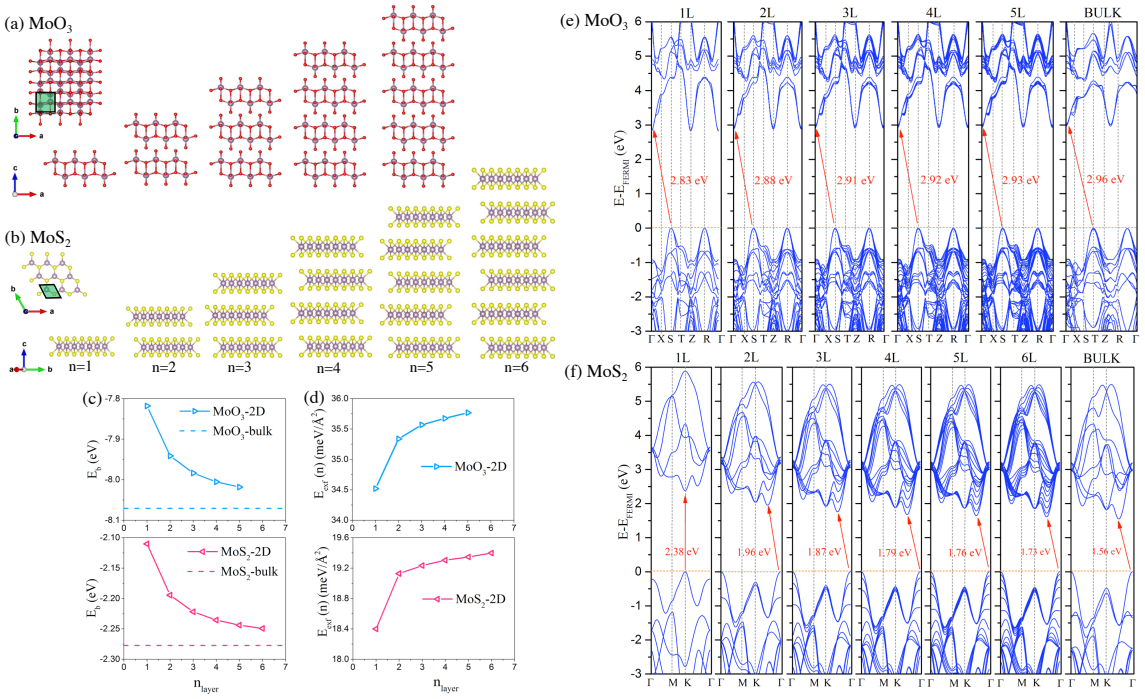

Figure S1. Top and side view of (3 × 3) supercell crystal structures (a, b), calculated layer depended binding energy (c), exfoliation energy (d) and electronic band structure (e, f) of the 1L-5L MoO_3 and 1L-6L MoS_2 systems. The purple, red and yellow balls in the geometrical models represent the Mo, O and S atoms, respectively. The binding energy and electronic band structure for 3D bulk phases are also presented.

MoO_3	a (Å)	b (Å)	d (Å)	T (Å)	E_b (eV)	E_{exf} (meV/ Å^2)	E_g (eV)	VB (eV)	CB (eV)	ε_{eff}
1L	3.706	3.910	---	6.401	-7.82	34.52	2.83	-9.39	-6.56	2.85
2L	3.710	3.927	0.601	6.391	-7.94	35.34	2.88	-9.4	-6.52	3.35
3L	3.711	3.930	0.590	6.388	-7.98	35.57	2.91	-9.41	-6.49	3.51
4L	3.712	3.934	0.585	6.386	-8.00	35.67	2.92	-9.41	-6.48	3.60
5L	3.713	3.936	0.584	6.385	-8.02	35.77	2.93	-9.41	-6.44	3.68
Bulk	3.72 (3.70)[25]	3.94 (3.96)[25]	0.580	6.370	-8.07 (-7.80)[26]	---	2.96 (3.0)[27]	---	---	4.3

Table S1. Calculated optimized lattice parameters (a and b), the average minimum distance between the O_t-planes of adjacent layers (d), the average thickness of each layer (T), binding energy (E_b) per MoO_3, the exfoliation energy (E_{exf}), the HSE06 electronic band gap (E_g), absolute valence and conduction band-edge positions (VB and CB) and effective high frequency dielectric constant (ε_{eff}) along out-of-plane direction of pristine 1L-5L MoO_3 structures. The simulated results for 3D bulk phase of α-MoO_3 are also presented. The values in parenthesis are the corresponding experimental values[25–27] (the simulated lattice parameter for MoO_3 bulk along the direction of the vdW interaction is 13.90 Å, agree well with the experimental data 13.87 Å[25]).

2D-MoS_2	*a* (Å)	*d* (Å)	*T* (Å)	E_b *(eV)*	E_{exf} *(meV/Å²)*	E_g *(eV)*	*VB(eV)*	*CB(eV)*	ε_{eff}
1L	3.154 (3.16)[28]	---	3.165	-2.110	18.40	2.38 (2.40)[29]	-6.36 (-7.46)[30]	-3.99 (-4.7)[30]	4.96
2L	3.155	2.971	3.166	-2.194	19.128	1.96 (2.10)[29]	-6.03 (-6.3)[30]	-4.07 (-4.4)[30]	5.86
3L	3.155	2.968	3.167	-2.222	19.233	1.87 (1.75)[29]	-5.92 (-6.0)[30]	-4.05 (-4.3)[30]	6.13
4L	3.156	2.966	3.167	-2.236	19.304	1.79	-5.88 (-5.6)[30]	-4.09 (-4.0)[30]	6.23
5L	3.156	2.964	3.168	-2.244	19.346	1.76	-5.86	-4.10	6.26
6L	3.156	2.962	3.169	-2.250	19.398	1.73	-5.85	-4.12	6.26
Bulk	3.16 (3.16)[31]	2.94	3.17	-2.28 (-2.81)[32]	---	1.56 (1.23)[33]	---	---	6.30

Table S2. Optimized lattice parameters (*a*), the average minimum distance between the S-planes of adjacent layers (*d*), the average thickness of each layer (*T*), binding energy (E_b) per MoS_2, the exfoliation energy (E_{exf}), the HSE06 electronic band gap (E_g), absolute valence and conduction band-edge position (VB and CB) and effective high frequency dielectric constant (ε_{eff}) along out-of-plane direction of pristine 1L-6L MoS_2 structures. The simulated results for 3D bulk phase of 2H-MoS_2 are also presented. The simulated lattice parameter for 2H-MoS_2 bulk along the direction of the vdW interaction is 12.28 Å, agree well with the experimental data 12.29 Å[31]. Note that the experimental band gap values are optical band gap.

S2.2. Absolute valence and conduction band position

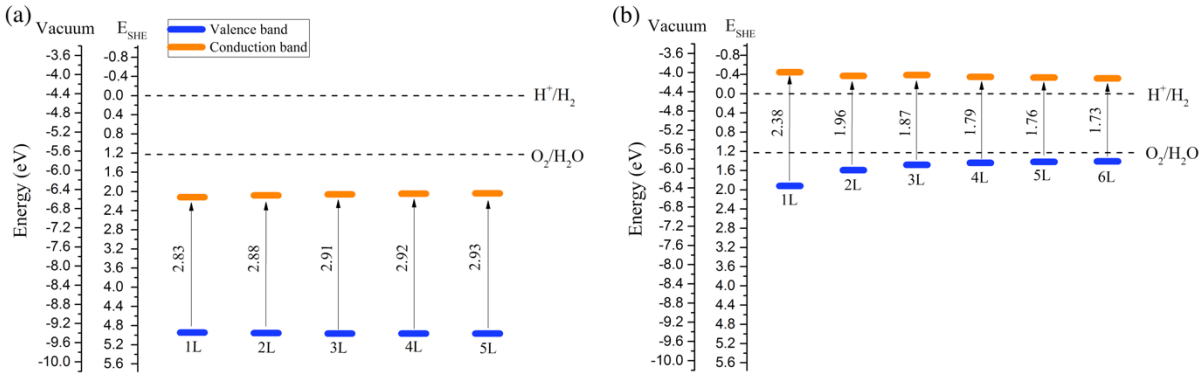

Figure S2. Calculated conduction and valence band-edge positions for 1L-5L MoO_3 (a) and 1L-6L MoS_2 (b) respect to vacuum level and standard hydrogen electrode. The lower edge of the conduction band (orange colour) and upper edge of the valence band (blue colour) are presented along with the band gap in electron volts. The dashed black lines indicate the water stability limits for hydrogen and oxygen evolution. The absolute potential of the standard hydrogen electrode was taken as 4.44 eV at a pH = 0.

S3. MoO_3/MoS_2 interface

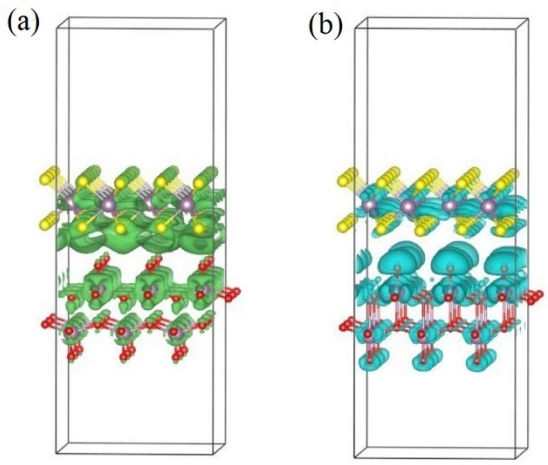

Fig. S3. Charge density difference Δρ = ρ(MoO_3/MoS_2) − ρ(MoO_3) − ρ(MoS_2) for MoO_3/MoS_2 heterojunction. Δρ is shown by isosurfaces bounding regions of electron accumulation at +1.2 × 10^{-4} e/Å^3 (a) and electron depletion at −1.2 × 10^{-4} e/Å^3 (b).

S4. S-doped 1L MoO_3 and O doped 1L MoS_2

S4.1. Structures and binding energies

To study the effects of sulfur doped SL MoO_3 and oxygen doped SL MoS_2 structures, different dopant concentrations were considered for both systems. To this aim, a host unit-cell structure of aforementioned systems was adopted for high dopant concentration levels while different size supercells (3×3) and (2×2) were used for low concentration levels. For S-doped SL MoO_3 and O-doped SL MoS_2, the maximum doping concentration is considered up to 33% and 100%, respectively. For each doping level, several configurations were tested and only the properties of the most stable ones are presented in this work.

To evaluate the stability of these structures, the binding energies per MoO_3 of S-doped SL MoO_3 supercell were computed as:

$$E_b = \left(\frac{E_{tot} - (n_{Mo}E_{Mo} + (\frac{1}{2})n_O E_{O_2} + n_S E_{S_\alpha})}{N} \right) \times 4 \quad (11)$$

and the binding energies of O-doped SL MoS_2 structures per MoS_2 were computed as

$$E_b = \left(\frac{E_{tot} - (n_{Mo}E_{Mo} + n_S E_{S\alpha} + (\frac{1}{2})n_O E_{O2})}{N} \right) \times 3 \quad (12)$$

where E_{tot} is the total energy per cell, E_i is the energy of the i-th individual elements in their respective ground states, n_i is the number of species i in the structure and N is the total number of atoms per cell. We used the conventional reference states, solid molybdenum, solid sulfur (α-sulfur) and isolated O_2 to compute the binding energies.

S concentration (%)	System	corresponding cell	corresponding figure	*k-point mesh*	*a* (Å)	*b* (Å)	E_b(eV)	E_g *(eV)*	ε_{eff}
0.0	MoO_3	unitcell	Fig. S6 (a)	12×12×1	3.706	3.910	-7.82	2.83	2.85
1.85	$MoS_{0.06}O_{2.94}$	(3 × 3)	Fig. S6 (b)	4×4×1	3.705	3.914	-7.70	2.40	2.93
4.16	$MoS_{0.12}O_{2.88}$	(2 × 2)	Fig. S6 (c)	6×6×1	3.705	3.915	-7.55	2.41	3.06
8.33	$MoS_{0.25}O_{2.75}$	(2 × 2)	Fig. S6 (d)	6×6×1	3.704	3.913	-7.29	2.44	3.24
8.33	$MoS_{0.25}O_{2.75}$	(2 × 2)	Fig. S6 (e)	6×6×1	3.704	3.913	-7.29	2.41	3.33
12.5	$MoS_{0.38}O_{2.62}$	(2 × 2)	Fig. S6 (f)	6×6×1	3.702	3.910	-7.02	2.42	3.52
12.5	$MoS_{0.38}O_{2.62}$	(2 × 2)	Fig. S6 (g)	6×6×1	3.710	3.905	-7.04	1.98	3.65
16.66	$MoS_{0.5}O_{2.5}$	(2 × 2)	Fig. S6 (h)	6×6×1	3.703	3.910	-6.76	2.48	3.79
16.66	$MoS_{0.5}O_{2.5}$	(2 × 2)	Fig. S6 (i)	6×6×1	3.715	3.910	-6.78	2.06	3.99
25	$MoS_{0.75}O_{2.25}$	(2 × 2)	Fig. S6 (j)	6×6×1	3.711	3.90	-6.25	2.41	4.16
33	$MoSO_2$	unitcell	Fig. S6 (k)	12×12×1	3.72	3.89	-5.75	2.51	4.49

Table S3. Different models, corresponding figures, *k*-point mesh, calculated optimized lattice parameters (*a* and *b*), binding energy (E_b) per MoO_3, the electronic band gap (E_g) and effective high frequency dielectric constant (ε_{eff}) along out-of-plane direction for the S-substituted SL MoO_3 for different concentrations.

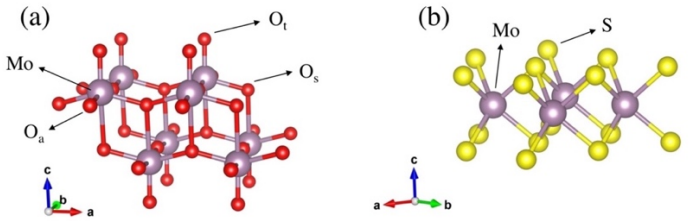

Figure S4. The (2×2) super-cells of (a) SL MoO_3 and (b) SL MoS_2. The unit-cell of SL MoO_3 includes 2Mo, 2 O_t (the apical oxygen atoms), 2 O_a (the corner-sharing oxygen atoms) and 2 O_s (the edge-sharing oxygen atoms), while the unit-cell of SL MoS_2 includes 1 Mo and 2 equivalent S. Color code as in Figure S1.

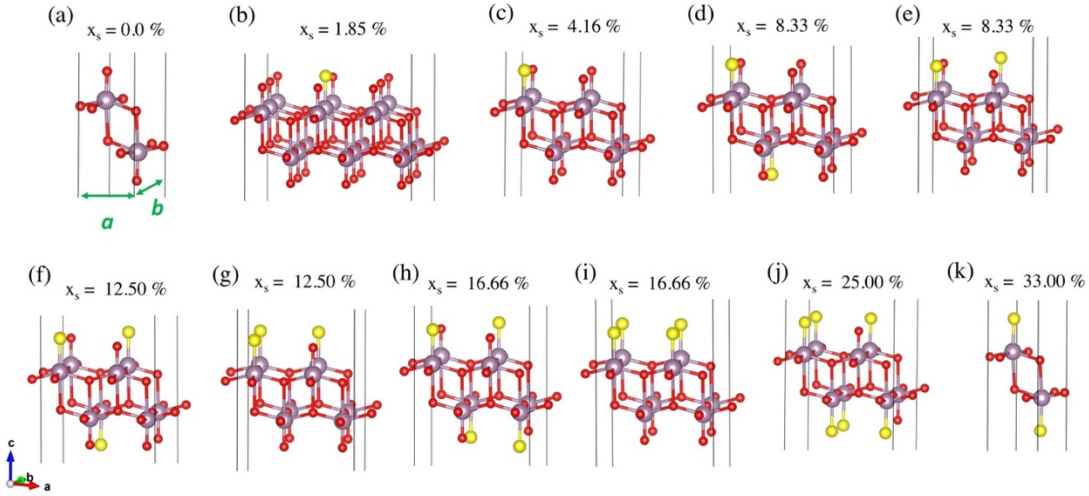

Figure S5. Optimized structures of S-doped SL MoO_3 for different concentrations (with increasing S content when going from (a) to (k)). Color code as in Figure S1. The lattice parameters of pristine structure are also shown with green arrows.

O concentration (%)	System	corresponding cell	corresponding figure	*k-point mesh*	*a* (Å)	E_b(eV)	E_g *(eV)*	ε_{eff}
0.0	MoS_2	unitcell	Fig. S7 (a)	12×12×1	3.155	-2.11	2.38	4.96
5.55	$MoO_{0.11}S_{1.89}$	(3 × 3)	Fig. S7 (b)	4×4×1	3.130	-2.26	2.41	4.67
11.11	$MoO_{0.22}S_{1.78}$	(3 × 3)	Fig. S7 (c)	4×4×1	3.115	-2.43	2.47	4.58
16.66	$MoO_{0.33}S_{1.67}$	(3 × 3)	Fig. S7 (d)	4×4×1	3.096	-2.58	2.39	4.42
16.66	$MoO_{0.33}S_{1.67}$	(3 × 3)	Fig. S7 (e)	4×4×1	3.093	-2.58	2.42	4.41
25	$MoO_{0.5}S_{1.5}$	(2 × 2)	Fig. S7 (f)	6×6×1	3.065	-2.82	2.25	4.68
25	$MoO_{0.5}S_{1.5}$	(2 × 2)	Fig. S7 (g)	6×6×1	3.056	-2.76	2.12	4.40
37.5	$MoO_{0.75}S_{1.25}$	(2 × 2)	Fig. S7 (h)	6×6×1	3.010	-3.17	2.19	4.42
50	MoOS	(2 × 2)	Fig. S7 (i)	6×6×1	2.960	-3.59	2.13	3.73
50	MoOS	unitcell	Fig. S7 (j)	12×12×1	2.987	-3.37	1.79	3.34
75	$MoO_{1.5}S_{0.5}$	(2 × 2)	Fig. S7 (k)	6×6×1	2.891	-4.40	2.00	3.07
100	MoO_2	unitcell	Fig. S7 (l)	12×12×1	2.818	-5.24	1.63	2.34

Table S4. Different models, corresponding figures, *k*-point mesh, calculated optimized lattice parameter (*a*), binding energy (E_b) per MoS_2, the electronic band gap (E_g) and effective high frequency dielectric constant (ε_{eff}) along out-of-plane direction for the O-substituted SL MoS_2 for different concentrations.

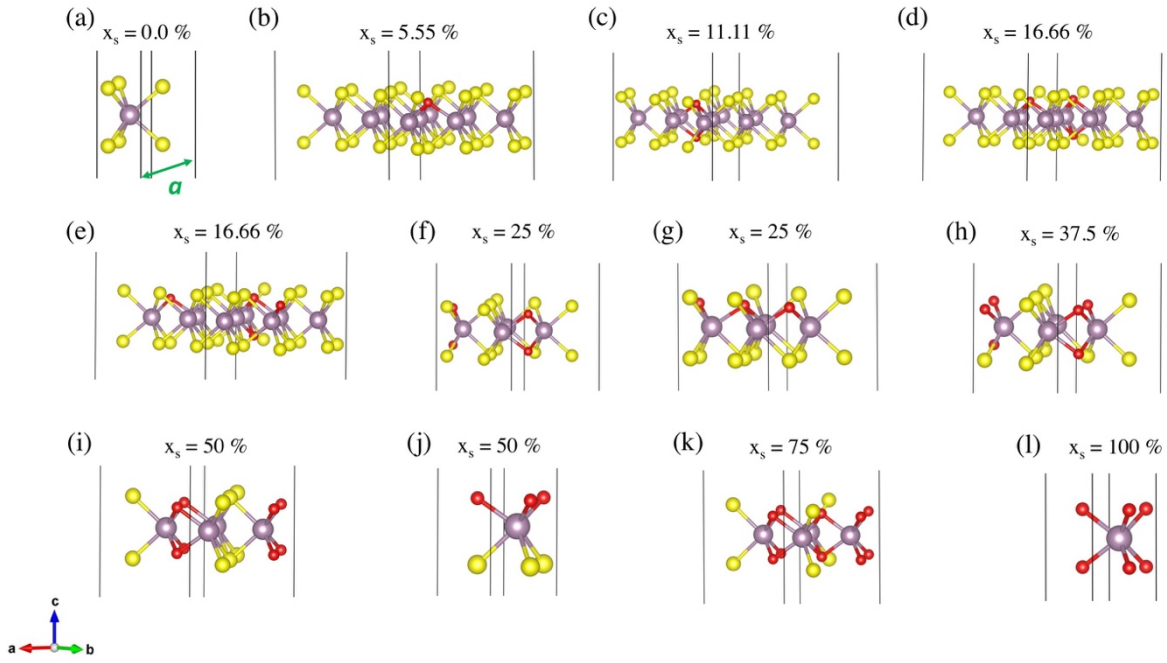

Figure S6. Optimized structures of O-doped SL MoS_2 for different concentrations (with increasing oxygen concentration when going from (a) to (l)). Color code as in Figure S1. The lattice parameters of pristine structure are also shown with green arrows.

S4.2. Thermodynamic analysis

For the more discerning of the stability of $SLMoO_{3-x}S_x$ and $MoS_{2-x}O_x$ compositions as a function of the number of S- or O-atoms exchanged in the MoO_3 and MoS_2 single-layer structures respectively, we calculate the Grand potential, Ω, assuming that the reservoir surrounding the solids is constituted from ideal gas phase mixtures of H_2S/H_2O (commonly used experimentally as sulfiding and oxidizing agents):

$MoO_3 + xH_2S = MoO_{(3-x)}S_x + xH_2O$ (13)

$MoS_2 + xH_2O = MoS_{(2-x)}O_x + xH_2S$ (14)

$$\Omega_{MoO_{3-x}S_x} = E_b(MoO_{3-x}S_x) - E_b(MoO_3) + xG^0_{f,T_0}(H_2O) - xG^0_{f,T_0}(H_2S) - xRT_0\ln\left[\frac{p(H_2S)}{p(H_2O)}\right] \quad (15)$$

$$\Omega_{MoS_{2-x}O_x} = E_b(MoS_{2-x}O_x) - E_b(MoS_2) + xG^0_{f,T_0}(H_2S) - xG^0_{f,T_0}(H_2O) - xRT_0\ln\left[\frac{p(H_2O)}{p(H_2S)}\right] \quad (16)$$

where E_b stands for the 0 K, binding energies of the different solids involved (neglecting vibrational and entropic contributions, see also supporting information), G^0_{f,T_0} stands for the Gibbs free energies of formation of H_2S and H_2O molecules (including thermal and entropic effects evaluated from NIST data base at T_0=298 K). So, for each value of x, we will plot the evolution of Ω_x as a function of the variable $\pm RT_0\ln\left[\frac{p(H_2O)}{p(H_2S)}\right]$ fixing the partial pressures of H_2S/H_2O in the reservoir assumed at T_0=298 K. It is worth to note that increasing T slightly diminishes (increases, respectively) the free enthalpy of oxidation (sulfidation, respectively) reaction (supplementary information). However, the main trends reported at ambient T are only very weakly affected.

Fig. S8 a and b illustrates the thermodynamic phase diagrams of substituted single-layer systems with respect to the pristine structures considering the H_2S/H_2O reservoir by using the Grand potential approach. It can be seen that for a $RT_0\ln\left[\frac{p(H_2S)}{p(H_2O)}\right]$ term greater than ~-0.27 eV, the pristine structure of SL MoO_3 becomes sulfided. For $RT_0\ln\left[\frac{p(H_2S)}{p(H_2O)}\right]$in the range between -0.27 and -0.19 eV, the structure with 4.16% S is the most stable. For $RT_0\ln\left[\frac{p(H_2S)}{p(H_2O)}\right]$in the range between -0.19 and -0.16 eV, the structure with 16.7% S is the most stable. For $RT_0\ln\left[\frac{p(H_2S)}{p(H_2O)}\right]$higher than -0.16 eV, system with 33% S is thermodynamically favored. By contrast, the oxidation of SL MoS_2 requires value of $RT_0\ln\left[\frac{p(H_2O)}{p(H_2S)}\right]$ as high as ~0.66 eV, which implies that the SL MoS_2 pristine system should remain stable while the structure with the highest O concentration (100%) should be favored.

Moreover, as an alternative pathway for the oxidation of SL MoS_2, we can also use O_2/SO_2:

$$MoS_2 + 3/2xO_2 = MoS_{(2-x)}O_x + xSO_2 \quad (17)$$

Neglecting the entropic changes for the solid phases, the Grand potential can be approximated as follows:

$$\Omega_{MoS_{2-x}O_x} = E_b(MoS_{2-x}O_x) - E_b(MoS_2) + xG^0_{f,T_0}(SO_2) - \frac{3}{2xG^0_{f,T_0}(O_2)} - xRT_0ln\left[\frac{p(O_2)^{\frac{3}{2}}}{p(SO_2)p_0^{\frac{1}{2}}}\right] \quad (18)$$

It can be easily shown that by using O_2 as oxidizer and SO_2 as a byproduct, reaction energies become exothermic and the thermodynamic diagram can be shifted to accessible reaction conditions (Fig. S8 c) which reveals that the chemical potential of O_2 required for oxidizing SL MoS_2 is very low in comparison to H_2O. This also shows that the full conversion of SL MoS_2 into SL MoO_3 is strongly exothermic process, which makes more difficult the control of the partial sulfidation state under O_2/SO_2 environment than under H_2O/H_2S.

By using equations S13 and S14 we can calculate the reaction energies for the most stable S-substituted SL MoO_3 and O-substituted SL MoS_2 nanostructures for different concentrations as depicted in Fig S8 d. In this figure, ΔE is the difference of 0K binding energy of the S-substituted SL MoO_3 and O-substituted SL MoS_2 systems with respect to DFT binding energies of H_2S and H_2O as reactants/products:

$$\Delta E = E_b(MoO_{3-x}S_x) - E_b(MoO_3) + xE_b(H_2O) - xE_b(H_2S) \quad (19)$$

ΔG is the difference of binding energy of the S-substituted SL MoO_3 and O-substituted SL MoS_2 systems with respect to experimental free energies (enthalpy and entropy) of H_2S and H_2O given by NIST thermodynamic database:

$$\Delta G = E_b(MoO_{3-x}S_x) - E_b(MoO_3) + xG_b(H_2O) - xG_b(H_2S) \qquad (20)$$

The reaction energies for the oxidation of ML MoS_2 are continuously increasing as a function of x, while the sulfidation energies of SL MoO_3 are continuously decreasing that reveals that the sulfidation process of SL MoO_3 is thermodynamically more favorable than the oxidation one SL MoS_2 when we consider H_2S/H_2O as reactants or products.

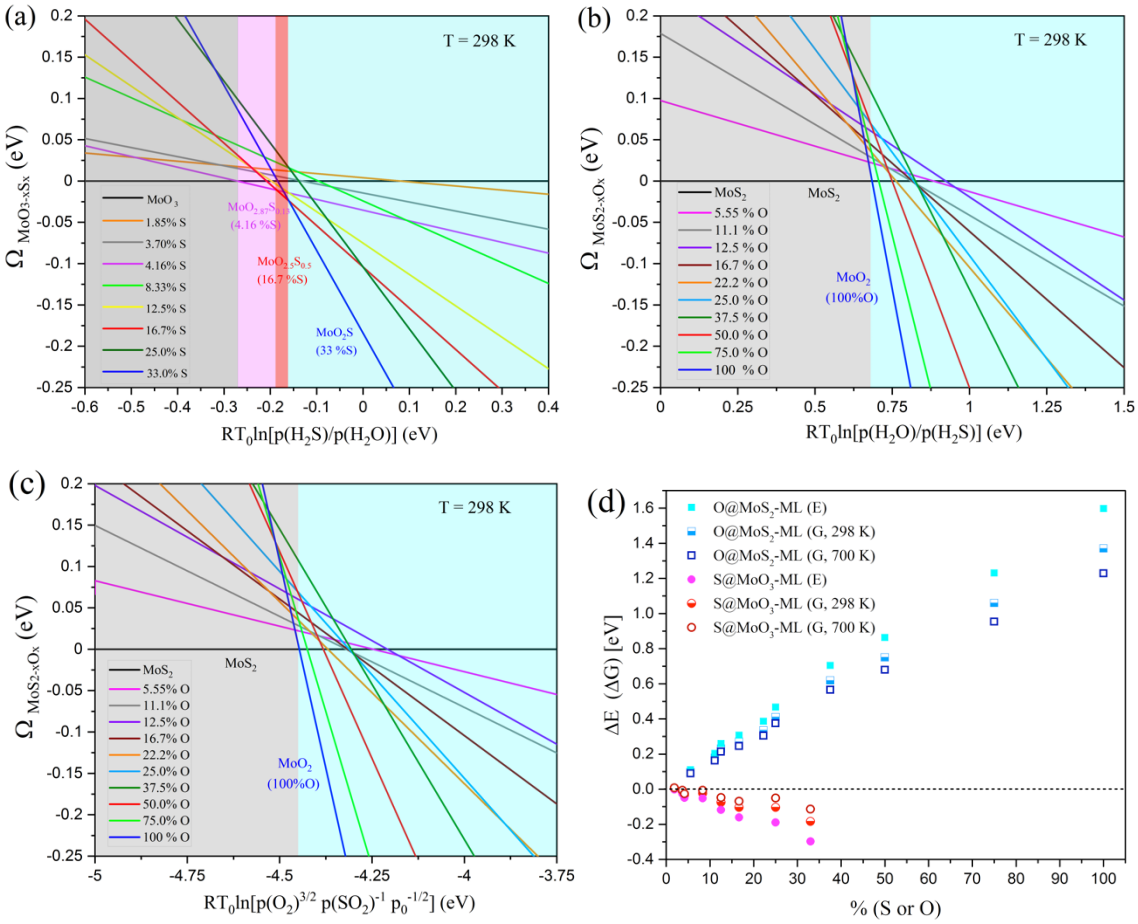

Figure S7. Thermodynamic phase stability of the S-substituted SL MoO_3 (a) and O-substituted SL MoS_2 (b) structures for different S- and O-concentrations with respect to pristine structures considering the H_2S/H_2O reservoir. (c) Thermodynamic phase stability of the O-substituted SL MoS_2 structures for different O-concentrations with respect to pristine structure considering O_2 reservoir and formation of solid sulfur. (d) The calculated reaction energy for the most stable S-substituted SL MoO_3 and O-substituted SL MoS_2 structures for different concentrations.

S4.3. Electronic and optical properties

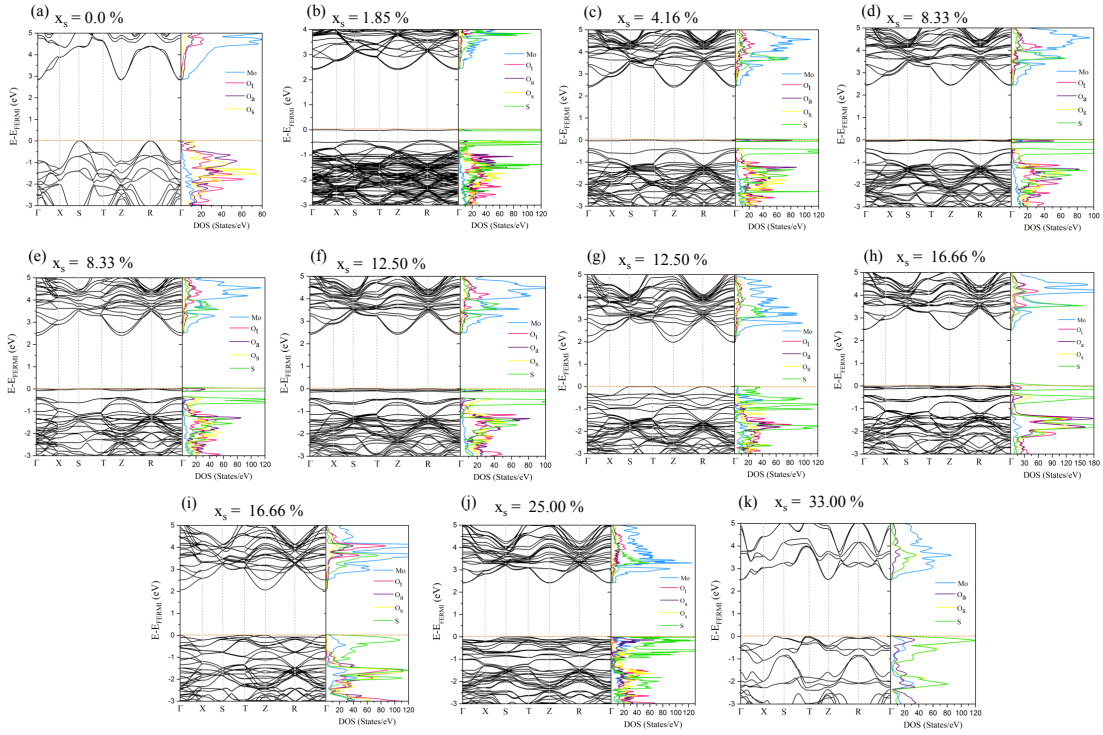

Figure S8. Band structure and PDOS of the most stable S-substituted SL MoO_3 structures for different concentrations calculated using HSE06. Labels from (a) to (k) corresponds to the structure of the Figure S5. The Fermi level is set to zero. The related structures are presented in Fig S6.

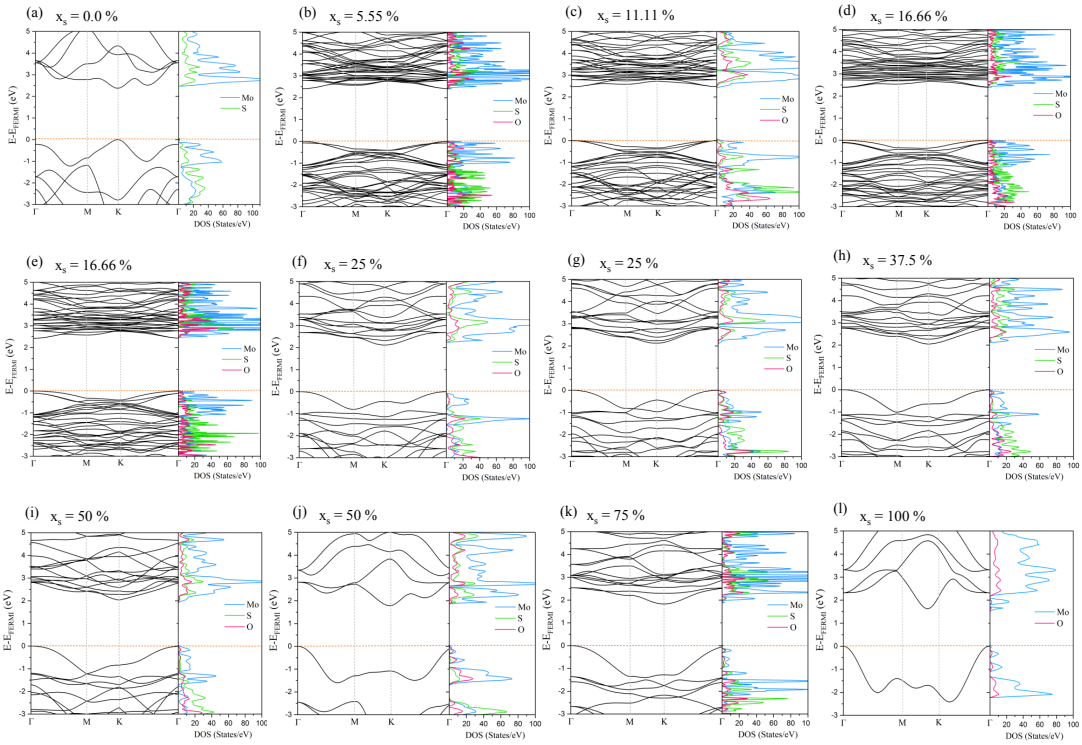

Figure S9. Band structure and PDOS of the most stable O-substituted SL MoS_2 structures for different concentrations calculated using HSE06. Labels from (a) to (l) corresponds to the structure of the Figure S6. The Fermi level is set to zero. The related structures are presented in Fig S7.

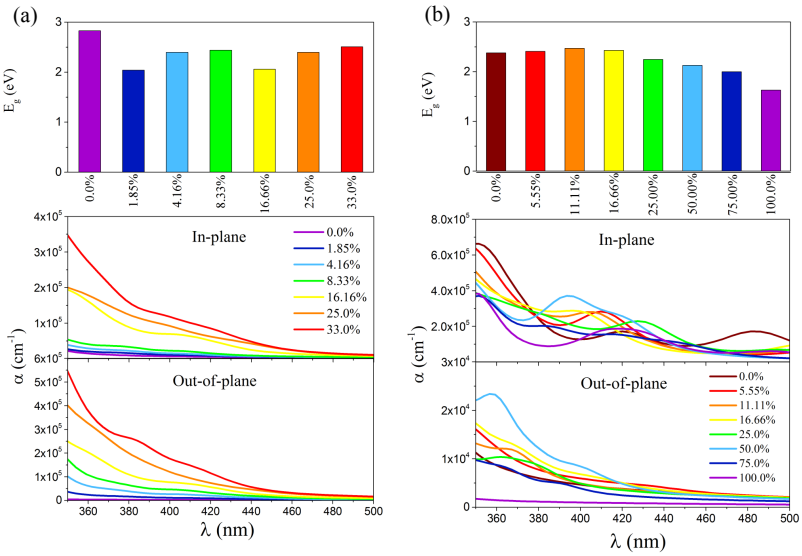

Figure S10. Computed electronic band gaps (in eV) and absorption coefficient (α, in cm^{-1}) along in-plane and out-of-plane of the most stable (a) S-doped MoO_3SL and (b) O-doped MoS_2SL for different S- and O-concentrations.

S4.4. High frequency dielectric profile $\varepsilon_\infty(z)$

The four-step procedure to calculate the high frequency dielectric profile $\varepsilon_\infty(z)$ of S doped SL MoO_3 and O doped SL MoS_2 is depicted in Fig. S13a and b.

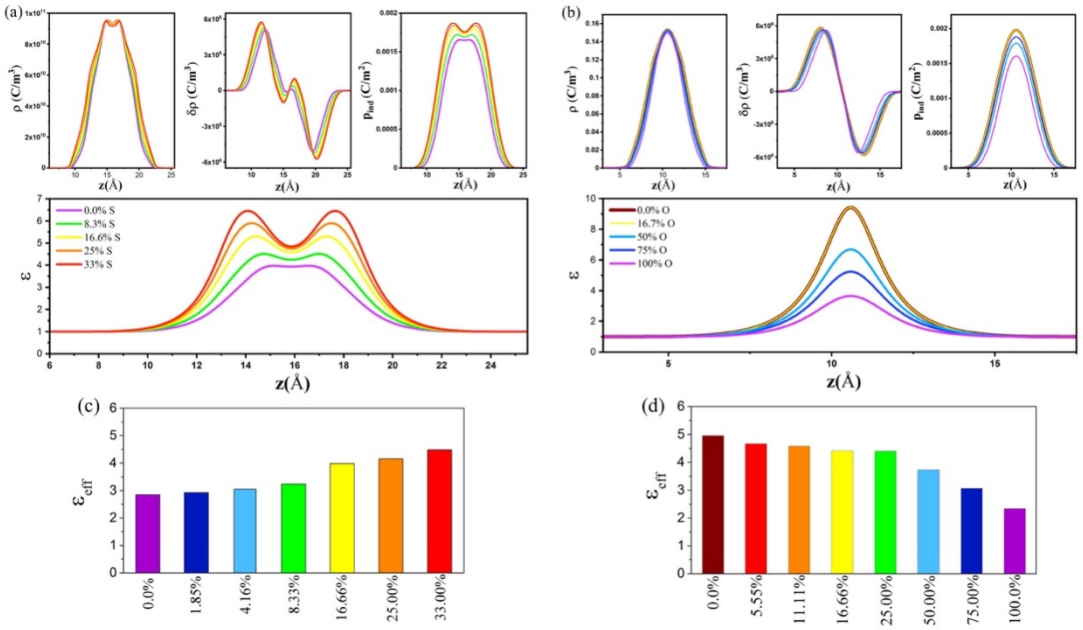

Figure S11 Four-step procedure to extract a dielectric constant profile along out-of-plane for (a) S-substituted SL MoO_3 and (b) O-substituted SL MoS_2 for different S- and O-concentrations. The effective dielectric constant along out-of-plane for (c) S-substituted SL MoO_3 and (d) O-substituted SL MoS_2 for different S- and O-concentrations.

S4.5. Absolute valence and conduction band position

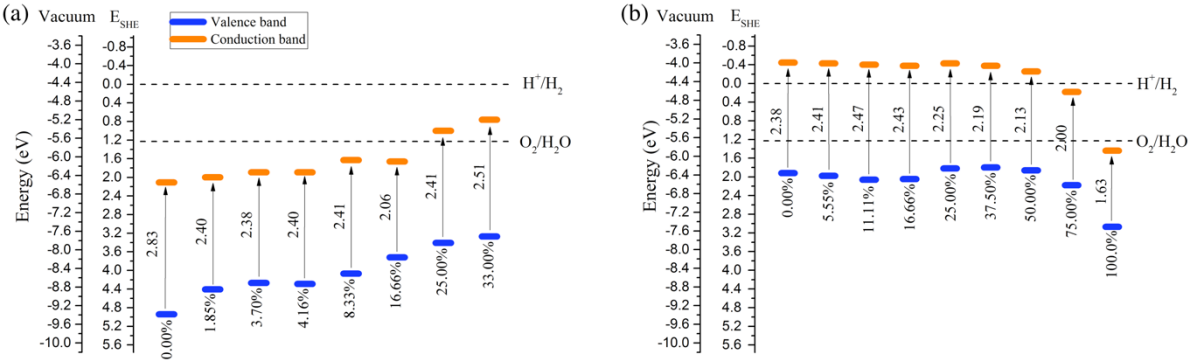

Figure S12. Calculated conduction and valence band-edge positions for (a) S-doped MoO_3SL and (b) O-doped MoS_2SL with respect to vacuum level and standard hydrogen electrode. The lower edge of the conduction band (orange colour) and upper edge of the valence band (blue colour) are presented along with the band gap in electron volts. The dashed black lines indicate the water stability limits for hydrogen and oxygen evolution. The absolute potential of the standard hydrogen electrode was taken as 4.44 eV at a pH = 0.

S5. MoS_xO_{3-x}/MoS_2 heterojunctions

To assess the most stable configuration, the interface binding energies are calculated, which are defined as:

$$E_{b(interface)} = (E_{composite} - E_{MoS_xO_{3-x}} - E_{MoS_2})/\mathcal{A} \quad (21)$$

where $E_{composite}$, $E_{MoSxO3\text{-}x}$ and E_{MoS2} are the total energies of MoS_xO_{3-x}/MoS_2 heterojunction, 2D MoS_xO_{3-x} layer and 2D MoS_2 layer, respectively. And $\mathcal{A}$ is the in-plane area of the heterojunction unit cell.

S concentration (%) into MoO_3 layer	System	corresponding figure	*d* (Å)	$E_{b(interface)}$ ($meV/Å^2$)	E_g (eV)	ε_{eff}
0.0	MoO_3/MoS_2	Fig. S16 (a)	2.86	-5.36	metallic	---
1.9	$MoS_{0.06}O_{2.94}/MoS_2$	Fig. S16 (b)	2.96	-6.51	metallic	---
3.75	$MoS_{0.11}O_{2.89}/MoS_2$	Fig. S16 (c)	3.00	-6.74	metallic	---
5.55	$MoS_{0.17}O_{2.83}/MoS_2$	Fig. S16 (d)	3.04	-7.74	0.15	3.85
		Fig. S16 (e)	3.14	-7.43	0.18	3.78
		Fig. S16 (f)	2.87	-6.28	metallic	----
9.26	$MoS_{0.28}O_{2.72}/MoS_2$	Fig. S16 (g)	3.18	-8.04	0.41	4.3
16.66	$MoS_{0.5}O_{2.5}/MoS_2$	Fig. S16 (h)	3.21	-8.35	0.75	4.44
		Fig. S16 (i)	2.88	-5.74	Metallic	---
		Fig. S16 (j)	3.17	-7.81	0.62	4.34
		Fig. S16 (k)	3.19	-8.04	0.63	4.37
33	$MoSO_2/MoS_2$	Fig. S16 (l)	3.23	-8.65	1.05	4.52

Table S5. Different models, corresponding figures, calculated interlayer distance (*d*), binding energy (E_b), the electronic band gap (E_g) and effective high frequency dielectric constant (ε_{eff}) along out-of-plane direction for the MoS_xO_{3-x}/MoS_2 for different S concentration into MoO_3 layer.

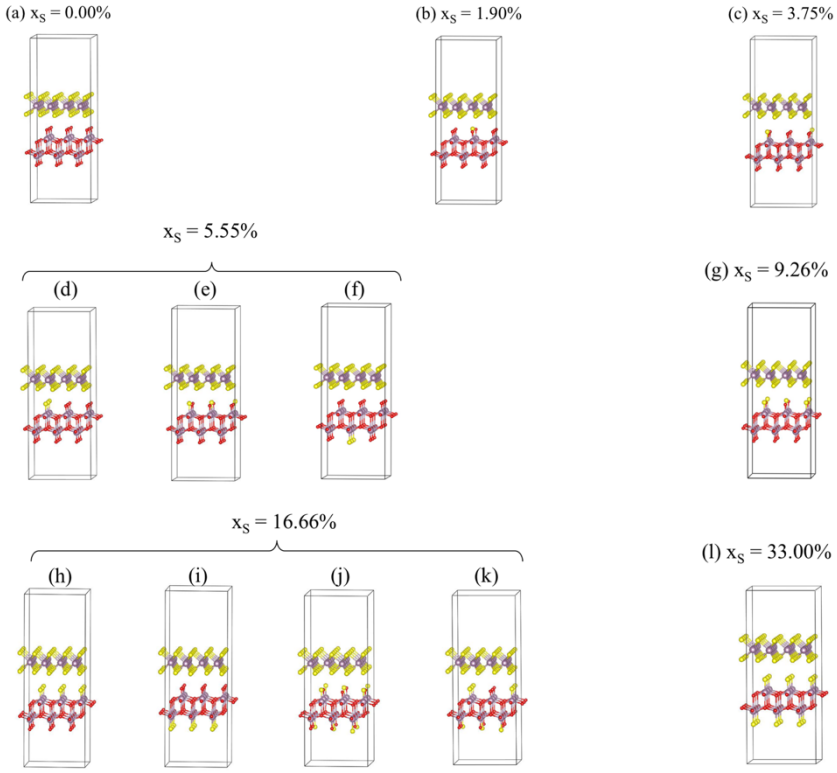

Figure S13. Optimized structures of S-doped MoO_3/MoS_2 interface for different concentrations (the increase of oxygen concentration in the MoO_3 layer follow the increase of the label from (a) to (l)). Color code as in Figure S1.

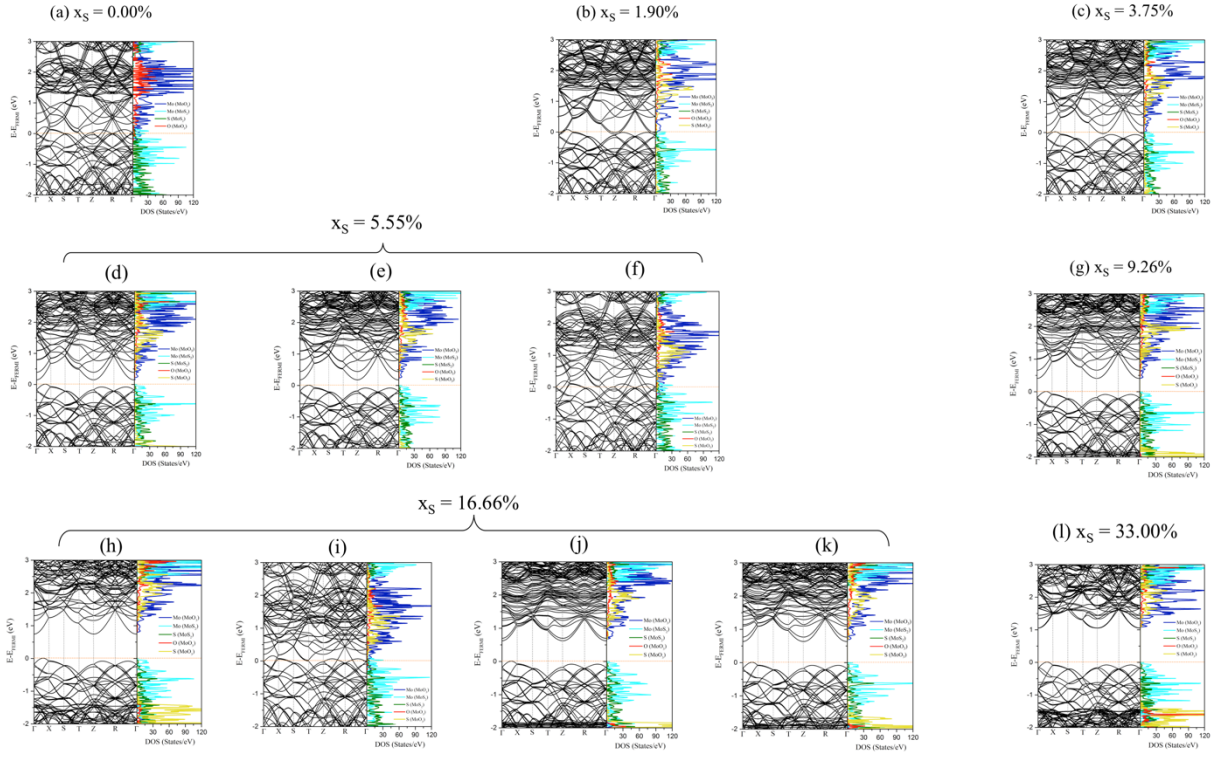

Figure S14. Band structure and PDOS of the of S-doped MoO_3/MoS_2 interface for different concentrations calculated using HSE06. The Fermi level is set to zero. Labels from (a) to (l) corresponds to the structure of the Figure S13. The related structures are presented in Fig S16.

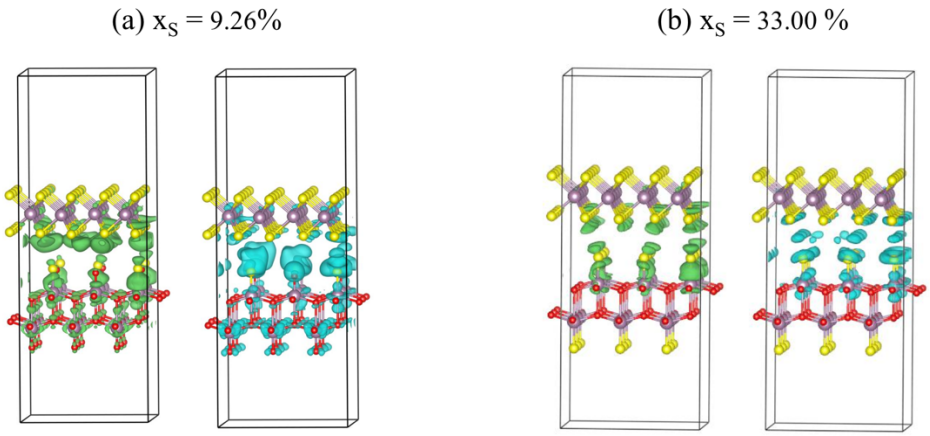

Figure S15. Charge density difference Δρ = ρ($MoO_{3-x}S_x/MoS_2$) − ρ($MoO_{3-x}S_x$) − ρ(MoS_2) for $MoO_{3-x}S_x/MoS_2$ heterojunction with x_S = 9.26% (a) and x_S = 33.00% (b). Δρ is shown by isosurfaces bounding regions of electron accumulation at +1.2 × 10^{-4} e/Å^3 (cyan) and electron depletion at −1.2 × 10^{-4} e/Å^3 (green).

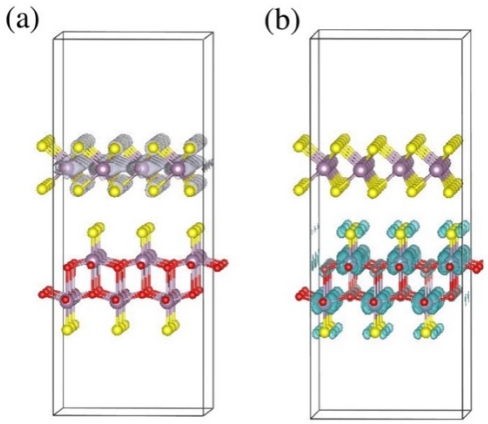

Figure S16. The partial charge densities of the VBM (a) and the CBM (b) for $MoSO_2$ /MoS_2 interface.

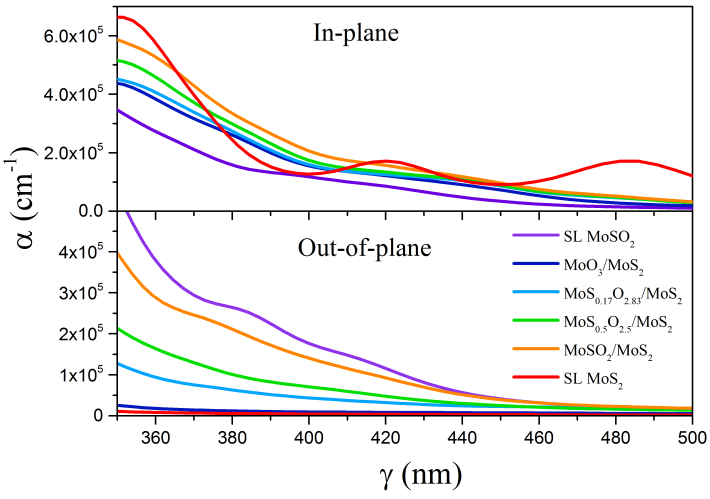

Figure S17. Absorption coefficient (α, in cm^{-1}) along in-plane and out-of-plane for SL $MoSO_2$, SL MoS_2, MoO_3/MoS_2 and MoS_xO_{3-x}/MoS_2 structures.

S6. Impact of increasing layers in MoS_xO_{3-x}/MoS_2 heterostructures

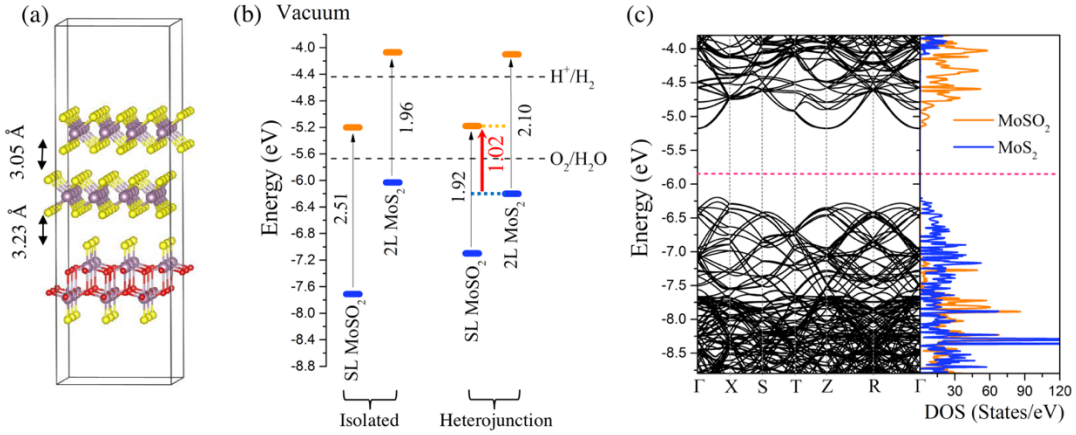

Figure S18. Optimized structure (a), conduction and valence band-edge positions respect to vacuum level (b), band structure and PDOS (c) for each layer for $MoSO_2$/2L-MoS_2 heterostructure.

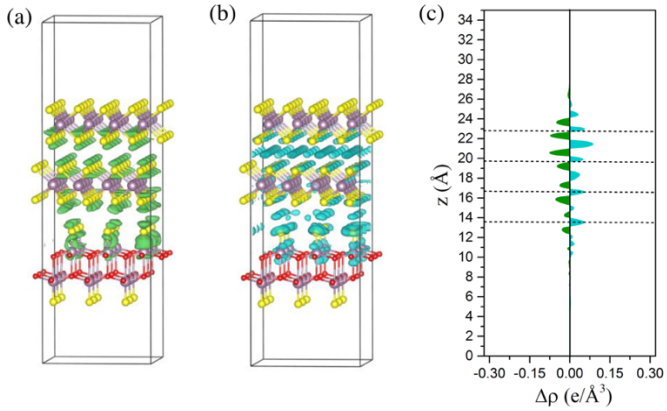

Figure S19. Charge density difference Δρ (a and b) and planar-averaged charge density difference ⟨Δρ(z)⟩ (c) for $MoSO_2$/2L-MoS_2 heterostructure. Δρ is shown by isosurfaces bounding regions of electron accumulation at $+1.2 \times 10^{-4}$ e/Å^3 (cyan) and electron depletion at -1.2×10^{-4} e/Å^3 (green).

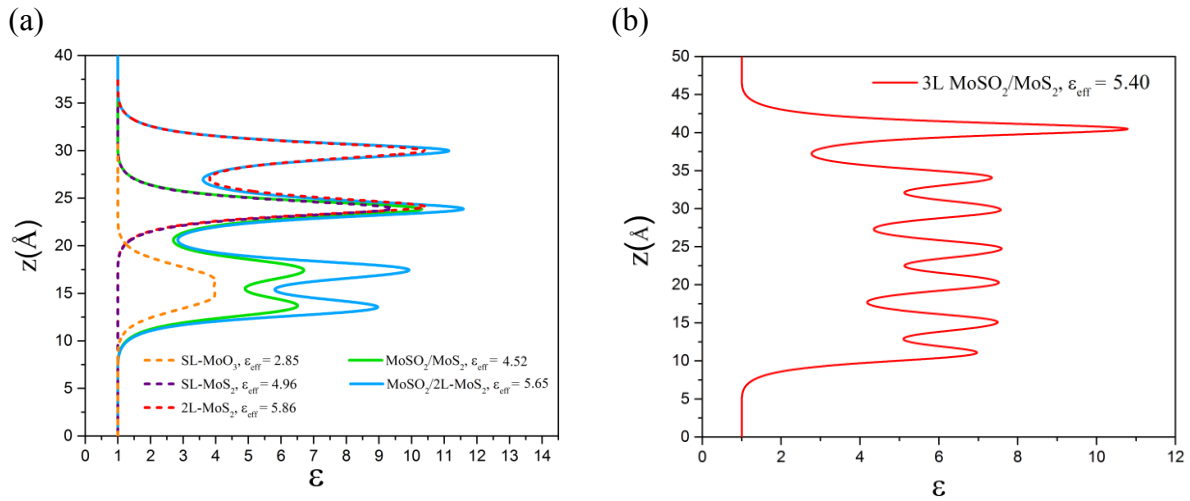

Figure S20. (a) Dielectric constant profile along out-of-plane for SL MoO_3, SL MoS_2, 2L MoS_2, $MoSO_2$/MoS_2 and $MoSO_2$/2L-MoS_2 heterostructures. The effective dielectric constant for each structure is also reported in the legend. (b) Dielectric constant profile along out-of-plane for 3L-$MoSO_2$/MoS_2 structures. The effective dielectric constant for each structure is also reported in this figure.

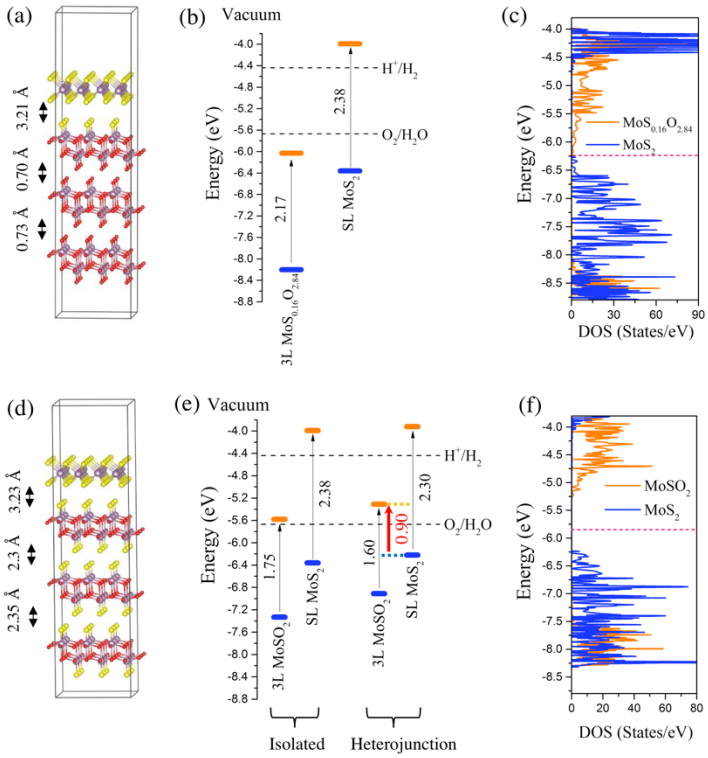

Figure S21. Optimized structure, conduction and valence band-edge positions respect to vacuum level and PDOS for each layer for 3L-$MoS_{0.17}O_{2.83}$/MoS_2 (a-c) and 3L-$MoSO_2$/MoS_2 (d-f) heterostructures.

S7. Atomic structures for VASP POSCAR file

S7.1. Atomic structure of S-doped MoO_3/MoS_2 in VASP POSCAR

MoO_3/MoS_2
1.0
11.7442188263 0.0000000000 0.0000000000
-0.0000917879 11.1179943081 0.0000000000
0.0000000000 0.0000000000 35.0000000000
Mo O S
34 54 32
Direct
0.811709762 0.582927644 0.326843709
0.499988377 0.331842035 0.502046227
0.250034809 0.331845194 0.502078831
0.999968827 0.331849605 0.502099991
0.875089109 0.082052000 0.502938807
0.374872506 0.081618406 0.502990901
0.124897622 0.082158603 0.502937257
0.749927819 0.331847668 0.502068162
0.144783393 0.916487038 0.326637238
0.478390664 0.916491032 0.326831460
0.477815866 0.582514226 0.326751530
0.144556403 0.583125651 0.326904714
0.477843165 0.250714481 0.326783001
0.144586489 0.250097662 0.326960534
0.811687112 0.250225067 0.326888233
0.810407043 0.916471362 0.326634049
0.856486738 0.749815822 0.240421519

0.625054479	0.081514150	0.503011167
0.189831406	0.749760389	0.240452662
0.624958336	0.581944764	0.502261937
0.874950707	0.581956029	0.502194166
0.523140728	0.750036240	0.240457997
0.999966383	0.831517220	0.503379524
0.250007898	0.831866145	0.503152192
0.499984324	0.832330942	0.502929807
0.749948859	0.832020521	0.503070116
0.124995507	0.581964850	0.502188563
0.375012189	0.581947803	0.502245367
0.856516838	0.083355673	0.240457773
0.189832896	0.083448857	0.240502879
0.523156106	0.083150946	0.240482435
0.523082078	0.416532665	0.240227595
0.856598377	0.416515768	0.240411103
0.189651921	0.416517675	0.240427539
0.992721081	0.916515827	0.321447909
0.327060848	0.916501880	0.320242584
0.659194112	0.916520834	0.319384336
0.824069500	0.252236128	0.375441700
0.488825172	0.256060094	0.375321120
0.488690495	0.577651262	0.375298142
0.824328303	0.581244409	0.375389516
0.153626025	0.582766652	0.375542819
0.159713820	0.915991843	0.375048101
0.489981085	0.915991426	0.375409991
0.817047775	0.916005909	0.375257552
0.993158817	0.583345950	0.320058316
0.153917372	0.250875860	0.375596672
0.659951329	0.583008230	0.320864111
0.511773050	0.082907803	0.192040801
0.326068968	0.249939740	0.320667744
0.006868987	0.749734759	0.247246057
0.511089504	0.416368783	0.191793367
0.326032877	0.583273470	0.320622176
0.845266700	0.083616398	0.192009673
0.178400770	0.083574772	0.192058384
0.673554659	0.750156045	0.247267127
0.340219051	0.749879718	0.247276574
0.673493028	0.416491687	0.246904641
0.340070128	0.416504741	0.247118846
0.006900989	0.416516066	0.247369960
0.006891152	0.083457604	0.247323036
0.673578918	0.083047137	0.247298047
0.340229601	0.083334975	0.247323766
0.511740804	0.750448346	0.192015454
0.178410187	0.749899149	0.192006990
0.845108807	0.749761343	0.191975161
0.845716417	0.416323990	0.191949517
0.166233212	0.249952570	0.256444752
0.499628335	0.249797344	0.256302416
0.177889854	0.416272014	0.191989884

0.832645357	0.583172143	0.256317496
0.833318472	0.916587532	0.256291628
0.832675159	0.249925122	0.256404668
0.499230951	0.916603565	0.256458312
0.498961180	0.083785631	0.311155260
0.832252085	0.083298251	0.310889721
0.165642723	0.416582316	0.310790360
0.166071832	0.916598976	0.256387800
0.498747170	0.416615814	0.309960902
0.498970628	0.749318898	0.311003566
0.832249463	0.749791324	0.310746223
0.499643147	0.583315372	0.256215602
0.165507004	0.749833703	0.310626537
0.659963250	0.250171781	0.320856333
0.993161261	0.249849230	0.320192814
0.166271374	0.583168507	0.256324977
0.832371294	0.416568220	0.310467988
0.165504888	0.083296172	0.310775518
0.375085324	0.917624235	0.548913062
0.999970376	0.168900847	0.548486590
0.499973387	0.168701306	0.548474252
0.749988854	0.168785945	0.548477829
0.125027865	0.417514712	0.547849596
0.375048071	0.417426616	0.547853649
0.624935031	0.417401850	0.547855794
0.874910116	0.417503238	0.547849119
0.999969900	0.665857553	0.548397362
0.499978870	0.666855991	0.548256159
0.749963701	0.666511834	0.548295736
0.125100732	0.917968035	0.549021363
0.249984711	0.168821752	0.548480690
0.250003844	0.666331172	0.548321486
0.124363825	0.917457044	0.457820505
0.625398755	0.917579710	0.457115293
0.624914110	0.917546988	0.548899174
0.999932706	0.166466564	0.456689000
0.250308782	0.166178361	0.456849247
0.500058472	0.165760800	0.457089931
0.749616861	0.166054204	0.456927836
0.124934852	0.417814076	0.456265897
0.875802577	0.917451918	0.457689226
0.374927551	0.417705715	0.456137598
0.875046313	0.417781055	0.456235021
0.999944627	0.668909431	0.456592292
0.250226676	0.669073462	0.456694931
0.500040770	0.669508517	0.456888497
0.749705493	0.669187486	0.456754506
0.374342501	0.917544723	0.457217187
0.625013351	0.417696923	0.456113935
0.874809623	0.917918503	0.548998177

S7.2. Atomic structure of S-doped $MoSO_2/MoS_2$ in VASP POSCAR

MoSO2/MoS2
1.0
11.6662597656 0.0000000000 0.0000000000
-0.0000461254 11.1740646361 0.0000000000
0.0000000000 0.0000000000 35.0000000000
Mo O S
34 36 50
Direct
0.808510721 0.916379809 0.325317770
0.475986212 0.916414440 0.325271070
0.142480209 0.916400611 0.325266153
0.475399524 0.582808912 0.325273126
0.142191634 0.582985997 0.325345099
0.809067726 0.582939982 0.325369954
0.475510150 0.250089824 0.325276792
0.142255917 0.249862000 0.325346470
0.809113443 0.249868155 0.325374454
0.857672870 0.749753535 0.240043283
0.190990135 0.749709964 0.239993975
0.524378419 0.749785721 0.239977837
0.190995872 0.416431516 0.239956304
0.857737124 0.416421384 0.239986062
0.191027269 0.083129004 0.240001976
0.857709885 0.083072759 0.240050241
0.524421751 0.083071925 0.239987209
0.374845386 0.081813663 0.524458170
0.124849215 0.082211226 0.524426460
0.875027359 0.082131177 0.524436712
0.250001192 0.331986934 0.523752630
0.624989331 0.081735320 0.524473846
0.999923885 0.331955731 0.523770690
0.749882579 0.832050443 0.524512291
0.499925107 0.832273841 0.524420559
0.249970198 0.831927836 0.524569035
0.999927163 0.831672788 0.524682939
0.874931097 0.582034886 0.523819566
0.624936163 0.581963480 0.523874104
0.374941319 0.581961393 0.523860216
0.124912061 0.582034051 0.523808837
0.749855697 0.331977308 0.523742855
0.499938726 0.332003504 0.523722231
0.524374723 0.416437894 0.239868358
0.990544021 0.916545033 0.320083052
0.009257318 0.749684215 0.246035412
0.166570038 0.583050311 0.253950536
0.833112597 0.583018064 0.254038721
0.499963045 0.249778539 0.253940940
0.166595578 0.249773934 0.253976047
0.833164930 0.249794632 0.254040927
0.675947785 0.749846518 0.246027187
0.009294863 0.083043396 0.246047705

0.009294075	0.416541040	0.246009722
0.675919294	0.416538566	0.245882720
0.342607081	0.416544646	0.245882362
0.499951869	0.583055139	0.253917783
0.675998509	0.082896940	0.246037409
0.342623115	0.083030000	0.245939821
0.342585653	0.749711931	0.245932981
0.499758601	0.916459560	0.253919691
0.166566610	0.916447401	0.254049152
0.323802322	0.583017111	0.319435954
0.657376647	0.582973778	0.319749802
0.990716219	0.582963228	0.319259435
0.324396819	0.916590273	0.319337904
0.657158315	0.916544914	0.318767250
0.833489776	0.916440070	0.253973305
0.657449722	0.249743402	0.319688290
0.990732014	0.249754161	0.319348067
0.500021279	0.749555707	0.311300129
0.166665524	0.749700189	0.311257273
0.323893070	0.249687508	0.319474906
0.500157475	0.416468292	0.311032832
0.166843638	0.416425496	0.311232060
0.833391905	0.416430980	0.311185449
0.500073969	0.083280317	0.311355740
0.166637048	0.083132587	0.311292976
0.833447278	0.083052784	0.311430156
0.833413661	0.749736845	0.311362147
0.177763313	0.083007708	0.179327533
0.490301788	0.915843785	0.385891616
0.159482524	0.915898621	0.385772109
0.817399144	0.915755749	0.386004299
0.488240570	0.578738391	0.385935247
0.154455319	0.582106888	0.386040926
0.824322760	0.580912888	0.385994762
0.488656402	0.254794598	0.385925233
0.154807776	0.251175016	0.386036366
0.823847830	0.252417862	0.386011660
0.844715178	0.749832869	0.179359838
0.511652410	0.749928594	0.179292604
0.177714080	0.749855936	0.179322377
0.844960093	0.416406453	0.179296792
0.511347473	0.416416645	0.179185852
0.177696496	0.416414917	0.179277286
0.844793141	0.083016634	0.179364458
0.511716068	0.082961999	0.179299697
0.749931812	0.168804899	0.569973290
0.749719977	0.669101000	0.478397518
0.499978364	0.669251442	0.478491217
0.250136167	0.668995559	0.478338778
0.999893010	0.668882549	0.478227019
0.874987483	0.417920768	0.477996677
0.624968588	0.417901188	0.477868319
0.374883503	0.417914331	0.477898180

0.124884181 0.417945653 0.478019446
0.749716163 0.166716784 0.478571206
0.499976188 0.166534767 0.478675187
0.250131220 0.166826129 0.478501409
0.999887288 0.167031214 0.478368968
0.124585815 0.917886019 0.479210556
0.374503791 0.917936683 0.478797525
0.625201941 0.917965472 0.478715301
0.875413656 0.917898595 0.479118556
0.874843836 0.918014944 0.570333838
0.374998838 0.917871892 0.570294738
0.124983951 0.918055832 0.570346832
0.749931216 0.667001426 0.569800436
0.499927461 0.667218447 0.569769502
0.249929652 0.666864455 0.569813967
0.999929249 0.666605830 0.569857061
0.874874353 0.417843223 0.569465458
0.624896049 0.417768002 0.569478810
0.374986678 0.417784393 0.569479287
0.124964103 0.417859674 0.569466233
0.499921083 0.168741301 0.569959402
0.249930874 0.168839678 0.569970191
0.999932468 0.168916538 0.569987297
0.624878466 0.917822778 0.570285439

S7.3. Atomic structure of S-doped $MoSO_2$/2L MoS_2 in VASP POSCAR

MoSO2/2L MoS2
1.0
11.6662597656 0.0000000000 0.0000000000
-0.0000461254 11.1740646361 0.0000000000
0.0000000000 0.0000000000 42.0000000000
Mo O S
50 36 82
Direct
0.808429062 0.916536570 0.269409746
0.475938261 0.916570902 0.269256145
0.142526180 0.916553020 0.269346029
0.475275040 0.582972705 0.269291341
0.142096564 0.583160341 0.269353092
0.808962822 0.583133876 0.269437075
0.475402027 0.250290781 0.269283950
0.142186224 0.250070691 0.269355059
0.809043050 0.250060201 0.269436598
0.857838750 0.749932826 0.198344305
0.191154569 0.749914169 0.198257670
0.524572134 0.749943852 0.198215052
0.191135749 0.416604728 0.198209509
0.857876539 0.416599214 0.198293656
0.191190869 0.083268322 0.198276341
0.857875705 0.083234355 0.198363662
0.524615884 0.083260968 0.198228925
0.374827594 0.083668776 0.435031384

0.124826670	0.084056281	0.434999049
0.874987185	0.083982803	0.435007334
0.249961004	0.333839864	0.434557229
0.624953985	0.083594233	0.435045481
0.999897003	0.333801597	0.434585482
0.749857843	0.833896458	0.435044825
0.499897301	0.834104061	0.434977889
0.249936894	0.833785594	0.435086399
0.999901056	0.833541751	0.435174763
0.874902248	0.583893239	0.434581906
0.624905944	0.583811164	0.434620231
0.374911785	0.583812773	0.434609473
0.124884576	0.583893776	0.434573501
0.749833524	0.333837718	0.434540480
0.499905914	0.333868265	0.434510052
0.749947369	0.666248024	0.583629608
0.499950141	0.666244268	0.583628476
0.249952212	0.666248858	0.583630621
0.999949336	0.666252494	0.583631337
0.874951184	0.416264951	0.583638549
0.624951243	0.416264832	0.583640635
0.374948144	0.416264921	0.583639503
0.124948867	0.416264921	0.583637357
0.749947846	0.166273534	0.583630264
0.499950260	0.166272625	0.583629489
0.249951810	0.166275322	0.583630860
0.999949336	0.166276544	0.583631814
0.374949574	0.916258574	0.583622098
0.874949694	0.916257143	0.583620965
0.624949336	0.916258991	0.583621442
0.124950096	0.916256607	0.583621502
0.524558246	0.416620076	0.198131040
0.990533769	0.916707695	0.265180856
0.009405996	0.749790967	0.203359634
0.166724786	0.583232462	0.209853262
0.833198547	0.583192766	0.210000247
0.500103831	0.249966547	0.209848315
0.166748613	0.249937564	0.209882215
0.833262086	0.249974445	0.210007414
0.676092029	0.750028014	0.203339353
0.009443047	0.083267108	0.203383967
0.009426985	0.416718900	0.203332394
0.676064551	0.416704029	0.203219727
0.342741728	0.416712523	0.203151301
0.500094473	0.583220899	0.209831372
0.676141500	0.083050057	0.203357056
0.342786551	0.083196290	0.203220293
0.342744172	0.749879122	0.203205660
0.499874085	0.916623950	0.209783465
0.166623890	0.916613698	0.210008889
0.323714048	0.583195746	0.264362395
0.657286704	0.583213687	0.264749259
0.990628183	0.583128393	0.264282525

0.324395359	0.916733146	0.264231056
0.657124639	0.916716218	0.263843536
0.833719432	0.916600943	0.209976286
0.657393575	0.249879763	0.264682531
0.990673482	0.249948680	0.264332473
0.499982148	0.749688327	0.257634938
0.166596815	0.749884069	0.257629484
0.323817492	0.249879405	0.264379919
0.500128984	0.416659862	0.257424682
0.166794270	0.416610897	0.257585377
0.833270550	0.416628957	0.257613778
0.500019610	0.083478928	0.257691294
0.166583478	0.083287992	0.257683486
0.833423257	0.083214648	0.257837147
0.833398700	0.749914169	0.257767141
0.177796081	0.083082899	0.147718161
0.489970863	0.915849209	0.319774270
0.160444722	0.915756345	0.319747776
0.816849411	0.915646553	0.319986582
0.487840831	0.578801751	0.319853544
0.154502854	0.582279921	0.319934577
0.824334621	0.580959082	0.319955409
0.488258392	0.255262643	0.319830090
0.154813543	0.251622856	0.319930136
0.823978841	0.252998233	0.319957107
0.844867229	0.750172257	0.147775859
0.512104213	0.750197649	0.147636607
0.177776635	0.750174344	0.147698104
0.845129311	0.416527152	0.147718310
0.511740565	0.416573405	0.147562817
0.177741379	0.416537255	0.147645280
0.844949126	0.083064929	0.147793174
0.512186170	0.083087936	0.147649065
0.249946088	0.330350101	0.621748745
0.999951839	0.330353439	0.621748745
0.874948084	0.080343492	0.621738732
0.624948680	0.080343641	0.621738315
0.499948323	0.330343634	0.621749759
0.749953866	0.330346256	0.621749640
0.124950580	0.580363393	0.621745825
0.374951869	0.080345489	0.621738911
0.374952048	0.580366671	0.621745825
0.124951273	0.080344997	0.621739089
0.624949038	0.580369115	0.621745706
0.999948740	0.830366194	0.621736169
0.874948204	0.580366075	0.621745944
0.749948025	0.830362797	0.621734917
0.499951303	0.830359042	0.621734619
0.249951392	0.830363035	0.621736109
0.749903619	0.170547292	0.472915560
0.499948502	0.830242932	0.545579791
0.749690473	0.670765460	0.396703035
0.499951124	0.670926213	0.396782249

0.250106096 0.670657456 0.396651506
0.999864936 0.670535326 0.396556526
0.875008583 0.419731617 0.396450460
0.624966800 0.419736356 0.396318585
0.374801844 0.419740498 0.396349043
0.124823429 0.419748694 0.396472424
0.749661565 0.168780521 0.396840870
0.499951631 0.168577373 0.396925151
0.250124574 0.168894336 0.396785647
0.999856651 0.169116423 0.396677196
0.124562107 0.919822752 0.397297710
0.374499410 0.919840336 0.396965623
0.625158250 0.919861257 0.396898508
0.875372291 0.919826448 0.397225022
0.249951407 0.830241084 0.545578897
0.999949813 0.830240786 0.545577347
0.874950647 0.580250204 0.545584857
0.624950707 0.580241084 0.545581758
0.374947250 0.580244303 0.545582294
0.124949396 0.580253720 0.545585394
0.749946058 0.330310732 0.545587957
0.499951482 0.330311507 0.545589089
0.249953181 0.330309242 0.545586288
0.999947429 0.330308944 0.545585334
0.874951661 0.080307111 0.545583427
0.624949932 0.080304123 0.545579791
0.374947995 0.080303460 0.545581102
0.124948330 0.080306955 0.545584559
0.749947608 0.830241382 0.545578718
0.874828756 0.919915438 0.473137319
0.374957889 0.919773877 0.473112345
0.124947734 0.919949710 0.473147154
0.749896705 0.669143915 0.472788006
0.499899209 0.669318855 0.472768724
0.249907017 0.669033647 0.472794622
0.999900520 0.668813884 0.472824872
0.874821842 0.419831514 0.472591549
0.624850214 0.419727951 0.472579092
0.374978334 0.419752061 0.472584218
0.124948360 0.419855833 0.472597480
0.499893546 0.170526847 0.472903013
0.249901652 0.170551777 0.472915739
0.999900877 0.170581877 0.472931057
0.624862909 0.919729888 0.473105699

S7.4. Atomic structure of 3L S-doped $MoSO_2/MoS_2$ in VASP POSCAR

3L S-doped $MoSO_2/MoS_2$
1.0
11.1740646362 0.0000000000 0.0000000000
-0.0001009765 11.6664762493 0.0000000000
0.0000000000 0.0000000000 52.0000000000
S Mo O

86 70 108
Direct
0.078577772 0.012404425 0.568690002
0.081204109 0.348506123 0.568803370
0.080409482 0.678850412 0.568664789
0.415271521 0.011202757 0.568793595
0.415577412 0.345667064 0.568605840
0.415258914 0.682347000 0.568662703
0.754042089 0.012225139 0.568676829
0.751240790 0.348235309 0.568776608
0.752337933 0.679009140 0.568663478
0.249353960 0.323110998 0.429615378
0.249881148 0.658008397 0.429562926
0.249702305 0.990826905 0.429675281
0.582537651 0.323061347 0.429600030
0.582217097 0.658100665 0.429549009
0.582265198 0.990880132 0.429661542
0.916119993 0.324479282 0.429574043
0.915930927 0.656624973 0.429515660
0.915970266 0.991478026 0.429505974
0.082220674 0.158257142 0.383785218
0.082661986 0.492608070 0.383560658
0.082206294 0.823318720 0.383535236
0.416249901 0.158790171 0.383876830
0.416201800 0.492627501 0.383631527
0.416274965 0.823212624 0.383604497
0.749902368 0.158374190 0.383776516
0.749514222 0.492601573 0.383547157
0.749887288 0.823379040 0.383509129
0.249953106 0.182777077 0.244755879
0.249895066 0.514153302 0.244557008
0.249849454 0.848802745 0.244488016
0.582378268 0.182715893 0.244739860
0.582394779 0.513970852 0.244531766
0.582493961 0.848871291 0.244462311
0.916303575 0.182291791 0.244643748
0.916267753 0.513703585 0.244454071
0.916294277 0.848642766 0.244378805
0.082898691 0.017029326 0.199796140
0.082965180 0.350369424 0.199817866
0.082886219 0.684271634 0.199770004
0.416402996 0.017012779 0.199824184
0.416447550 0.350340784 0.199838907
0.416442215 0.684407055 0.199801520
0.749707639 0.016929923 0.199807733
0.749610424 0.350383669 0.199829027
0.749703646 0.684167743 0.199780494
0.249905661 0.326382428 0.060774252
0.249967083 0.660007894 0.060721930
0.250100851 0.994694769 0.060777489
0.582632899 0.326427490 0.060771700
0.582545638 0.659981072 0.060719423
0.582470000 0.994634211 0.060776811

0.916551650	0.326420128	0.060736254
0.916551471	0.660275936	0.060675364
0.916475832	0.994786978	0.060744975
0.168453693	0.752209485	0.693384707
0.668212354	0.752436280	0.631952405
0.668470025	0.502249777	0.631833315
0.668330610	0.252036005	0.631927371
0.668072701	0.002214736	0.632035375
0.419255406	0.876999199	0.632017374
0.419197947	0.626807332	0.632254481
0.419180632	0.377487719	0.632324815
0.419232458	0.127603844	0.632076979
0.170124725	0.752426684	0.631850302
0.169942290	0.502237439	0.631751299
0.170022920	0.252029598	0.631829679
0.170228347	0.002212759	0.631923020
0.919158995	0.127269700	0.631598771
0.919166565	0.377231330	0.631669044
0.919155300	0.627149940	0.631632745
0.919156432	0.877211392	0.631569028
0.919066846	0.877213120	0.693231702
0.919129670	0.377234757	0.693226516
0.919066310	0.127173319	0.693248034
0.669892728	0.752212584	0.693488538
0.669968963	0.502255142	0.693503022
0.669886589	0.252242535	0.693508387
0.669817984	0.002213239	0.693494856
0.419080168	0.877245009	0.693652689
0.419248223	0.627309799	0.693673432
0.419269294	0.377196848	0.693688989
0.419102192	0.127160028	0.693667054
0.168128207	0.502261758	0.693423808
0.168312758	0.252247781	0.693411529
0.168627679	0.002206784	0.693379760
0.919131815	0.627273023	0.693211198
0.082357593	0.026474450	0.527904153
0.082496263	0.359895885	0.527937591
0.082478724	0.693062007	0.527850270
0.415952265	0.026068250	0.527982652
0.416006029	0.359792888	0.527854979
0.415987819	0.693093061	0.527823031
0.749588788	0.026414841	0.527901530
0.749492109	0.359830022	0.527920663
0.749564946	0.693013012	0.527852595
0.249247044	0.310642958	0.470437497
0.249401882	0.644197345	0.470366359
0.249367818	0.977396429	0.470478803
0.582693458	0.310633749	0.470428348
0.582608998	0.644197404	0.470355839
0.582553744	0.977414906	0.470470726
0.916014135	0.310866296	0.470392346
0.915974319	0.644070625	0.470347583
0.915963054	0.977606833	0.470321447

0.082756110	0.144877389	0.342977554
0.082754970	0.478310138	0.342763603
0.082768023	0.811392128	0.342694253
0.416198850	0.144967705	0.343067765
0.416179776	0.478379458	0.342824936
0.416183919	0.811469436	0.342771083
0.749540031	0.144927084	0.342963278
0.749547720	0.478353888	0.342745602
0.749536157	0.811440527	0.342670083
0.249605790	0.195139557	0.285575509
0.249562159	0.528343141	0.285352677
0.249582455	0.861807585	0.285296708
0.582770467	0.195158631	0.285560101
0.582776189	0.528312266	0.285326719
0.582784891	0.861823976	0.285276115
0.916202486	0.194961250	0.285466343
0.916183114	0.528198540	0.285261512
0.916206837	0.861569405	0.285184145
0.082985297	0.030575652	0.158992156
0.082995206	0.363934398	0.159016520
0.082981847	0.697317302	0.158961192
0.416378319	0.030592537	0.159039050
0.416387975	0.363986909	0.159043252
0.416387498	0.697337508	0.158989727
0.749719977	0.030556152	0.159007967
0.749707758	0.363934815	0.159022793
0.749727368	0.697282255	0.158968955
0.249703363	0.314359516	0.101625673
0.249720499	0.647653103	0.101566277
0.249738678	0.981166661	0.101606652
0.583011091	0.314354509	0.101624556
0.582993388	0.647640288	0.101566084
0.582972944	0.981142879	0.101613179
0.916378975	0.314405590	0.101590209
0.916376173	0.647761583	0.101519749
0.916367650	0.981227040	0.101569019
0.083272032	0.377250195	0.662472963
0.083182387	0.127229810	0.662507713
0.083192475	0.877215862	0.662502706
0.333147913	0.252177030	0.662889361
0.083268628	0.627220511	0.662465036
0.333475649	0.002222849	0.662796557
0.833197653	0.752287745	0.662432134
0.833147764	0.502237141	0.662449718
0.833187640	0.252156317	0.662462950
0.833231449	0.002216549	0.662441552
0.582976460	0.877174854	0.662833214
0.583329320	0.627147377	0.662808955
0.583403230	0.377299070	0.662811577
0.583041608	0.127311528	0.662838101
0.333279908	0.752268493	0.662840009
0.332947612	0.502232015	0.662938952
0.082580194	0.178122833	0.524097681

0.082481012	0.511264861	0.523742974
0.082460321	0.844674349	0.523983777
0.416132897	0.177696779	0.523981869
0.416122556	0.511547267	0.524028659
0.416092426	0.844470620	0.523609996
0.749250710	0.178040177	0.524077535
0.749368787	0.511238098	0.523753881
0.749413252	0.844591200	0.523936212
0.249328479	0.001860966	0.518529058
0.249315366	0.335185558	0.518463254
0.249148473	0.668397725	0.518400609
0.582591414	0.001808500	0.518552661
0.582665086	0.335177720	0.518451273
0.582819879	0.668415427	0.518440604
0.915995002	0.001871413	0.518265367
0.915992796	0.334928751	0.518430591
0.916031957	0.668555439	0.518297732
0.082583889	0.002136653	0.479945779
0.082648754	0.335445821	0.479964584
0.082601115	0.668749750	0.479851604
0.415996224	0.002052493	0.480043441
0.415996164	0.335297406	0.479985178
0.416057497	0.668686152	0.479920864
0.749321103	0.002137978	0.479966998
0.749308586	0.335328072	0.479961753
0.749307334	0.668717802	0.479882270
0.249142379	0.159186289	0.474521577
0.249306738	0.492587268	0.474315464
0.249266922	0.825862408	0.474436402
0.582644820	0.159194916	0.474521935
0.582563996	0.492574394	0.474306524
0.582568526	0.825879931	0.474443704
0.916135430	0.159400150	0.474321216
0.916065574	0.492550969	0.474361420
0.916073024	0.825977385	0.474217951
0.082623005	0.326761007	0.338935018
0.082743667	0.660127401	0.338528037
0.082675315	0.993344069	0.338968813
0.416302055	0.326880217	0.339001983
0.416256487	0.660064697	0.338603854
0.416305840	0.993542552	0.339131624
0.749603331	0.326814055	0.338905811
0.749517679	0.660108805	0.338521451
0.749551237	0.993433952	0.338957965
0.249490395	0.169615224	0.333502620
0.249478951	0.502982855	0.333251417
0.249499142	0.836426497	0.333199382
0.582846522	0.169666678	0.333462924
0.582837522	0.503059030	0.333236217
0.582821488	0.836400449	0.333177865
0.916177690	0.169639602	0.333361775
0.916185319	0.503109396	0.333128482
0.916191757	0.836409569	0.333072215

0.082839422	0.170227498	0.295109421
0.082813263	0.503543615	0.294874370
0.082850963	0.836966634	0.294798970
0.416197538	0.170201033	0.295211554
0.416196346	0.503548265	0.294938624
0.416199386	0.837064445	0.294911504
0.749528527	0.170211628	0.295090020
0.749523818	0.503546298	0.294855922
0.749515176	0.836966217	0.294784188
0.249507993	0.013214497	0.289356142
0.249595776	0.346568793	0.289607227
0.249575734	0.679842591	0.289206773
0.582731724	0.013178686	0.289317906
0.582694411	0.346605748	0.289570987
0.582709670	0.679843783	0.289159358
0.916328549	0.013107685	0.289214253
0.916267335	0.346386760	0.289436370
0.916280031	0.679713428	0.289045215
0.082888432	0.182081625	0.154998437
0.082902610	0.515487194	0.155035838
0.082881100	0.848796129	0.154930353
0.416482866	0.182101056	0.155041918
0.416501164	0.515538454	0.155086040
0.416509002	0.848818600	0.154964998
0.749740124	0.182082623	0.155035570
0.749710321	0.515494764	0.155055210
0.749729633	0.848782063	0.154954284
0.249714121	0.339293510	0.149520189
0.249686077	0.672692418	0.149430528
0.249684423	0.005970167	0.149491772
0.583027124	0.339261264	0.149514288
0.583047032	0.672674894	0.149434432
0.583045125	0.005991073	0.149493739
0.916358292	0.339291781	0.149482235
0.916371584	0.672631025	0.149382129
0.916367352	0.005943482	0.149436891
0.083044350	0.005848155	0.110985912
0.082999110	0.339296848	0.111004062
0.083024204	0.672592342	0.110930711
0.416388750	0.005897942	0.111048236
0.416375697	0.339244932	0.111039415
0.416380882	0.672570288	0.110984959
0.749650240	0.005898173	0.111002095
0.749718964	0.339316905	0.111009255
0.749687374	0.672639251	0.110932320
0.249695048	0.162925884	0.105759993
0.249719828	0.496176064	0.105676204
0.249741942	0.829606950	0.105586097
0.582905352	0.162918419	0.105752587
0.582906187	0.496164083	0.105674863
0.582881570	0.829566598	0.105577670
0.916491210	0.162965670	0.105728082
0.916471899	0.496248156	0.105596349

0.916468084 0.829662025 0.105525427

References

(1) Cora, F.; Patel, A.; Harrison, N.; Roetti, C.; Catlow, C. An Ab Initio Hartree – Fock Study of a-MoO3. *J. Mater. Chem.* **1997**, *7*, 959–967.

(2) Lichanot, A.; Aprà, E.; Dovesi, R. Quantum Mechnical Hartree-Fock Study of the Elastic Properties of Li2S and Na2S. *Phys. Stat. Sol.* **1993**, *177*, 157–163.

(3) Valenzano, L.; Torres, F. J.; Doll, K.; Pascale, F.; Zicovich-Wilson, C. M.; Dovesi, R. Ab Initio Study of the Vibrational Spectrum and Related Properties of Crystalline Compounds; the Case of CaCO3 Calcite. *Z. Phys. Chem.* **2006**, *220*, 893–912.

(4) Perdew, J.; Burke, K.; Ernzerhof, M. Generalized Gradient Approximation Made Simple. *Phys. Rev. Lett.* **1996**, *77*, 3865–3868.

(5) Grimme, S.; Antony, J.; Ehrlich, S.; Krieg, H. A Consistent and Accurate Ab Initio Parametrization of Density Functional Dispersion Correction (DFT-D) for the 94 Elements H-Pu. *J. Chem. Phys.* **2010**, *132*, 154104.

(6) Shahrokhi, M.; Raybaud, P.; Le Bahers, T. On the Understanding of the Optoelectronic Properties of S-Doped MoO3 and O-Doped MoS2 Bulk Systems: A DFT Perspective. *J. Mater. Chem. C* **2020**, *8*, 9064–9074.

(7) Dovesi, R.; Erba, A.; Orlando, R.; Zicovich-Wilson, C. M.; Civalleri, B.; Maschio, L.; Rérat, M.; Casassa, S.; Baima, J.; Salustro, S.; et al. Quantum-Mechanical Condensed Matter Simulations with CRYSTAL. *WIREs Comput Mol Sci.* **2018**, *8*, 1–36.

(8) Heyd, J.; Scuseria, G. E.; Ernzerhof, M. Erratum: "Hybrid Functionals Based on a Screened Coulomb Potential" [J. Chem. Phys. 118, 8207 (2003)]. *J. Chem. Phys.* **2006**, *124*, 219906.

(9) Kresse, G.; Furthmüller, J. Efficient Iterative Schemes for Ab Initio Total-Energy Calculations Using a Plane-Wave Basis Set. *Phys. Rev. B* **1996**, *54*, 11169–11186.

(10) Kresse, G.; Furthmüller, J. Efficiency of Ab-Initio Total Energy Calculations for Metals and Semiconductors Using a Plane-Wave Basis Set. *Comput. Mater. Sci.* **1996**, *6*, 15–50.

(11) Kresse, G.; Hafner, J. Ab Initio Molecular Dynamics for Liquid Metals. *Phys. Rev. B* **1993**, *47*, 558–561.

(12) Blöchl, P. E. Projector Augmented-Wave Method. *Phys. Rev. B* **1994**, *50*, 17953–17979.

(13) Wooten, F. *Optical Properties of Solids*; 2013.

(14) Giustino, F.; Umari, P.; Pasquarello, A. Dielectric Discontinuity at Interfaces in the Atomic-Scale Limit: Permittivity of Ultrathin Oxide Films on Silicon. *Phys. Rev. Lett.* **2003**, *91*, 267601.

(15) Sapori, D.; Kepenekian, M.; Pedesseau, L.; Katan, C.; Even, J. Quantum Confinement and Dielectric Profiles of Colloidal Nanoplatelets of Halide Inorganic and Hybrid Organic-Inorganic Perovskites. *Nanoscale* **2016**, *8*, 6369–6378.

(16) Even, J.; Pedesseau, L.; Kepenekian, M. Electronic Surface States and Dielectric Self-Energy Profiles in Colloidal Nanoscale Platelets of CdSe. *Phys. Chem. Chem. Phys.* **2014**, *16*, 25182–25190.

(17) Junquera, J.; Cohen, M. H.; Rabe, K. M. Nanoscale Smoothing and the Analysis of Interfacial Charge and Dipolar Densities. *J. Phys. Cond. Mat.* **2007**, *19*, 213203.

(18) Giustino, F.; Pasquarello, A. Theory of Atomic-Scale Dielectric Permittivity at Insulator Interfaces. *Phys. Rev. B* **2005**, *71*, 1–13.

(19) Ramprasad, R.; Shi, N. Dielectric Properties of Nanoscale HfO_2 Slabs. *Phys. Rev. B* **2005**, *72*, 1–4.

(20) Shi, N.; Ramprasad, R. Dielectric Properties of Ultrathin SiO_2 Slabs. *Appl. Phys. Lett.*

2005, *87*, 262102.
(21) Shi, N.; Ramprasad, R. Atomic-Scale Dielectric Permittivity Profiles in Slabs and Multilayers. *Phys. Rev. B* **2006**, *74*, 1–7.
(22) Soler, J. M.; Artacho, E.; Gale, J. D.; García, A.; Junquera, J.; Ordejón, P.; Sánchez-Portal, D. The SIESTA Method for Ab Initio Order-N Materials Simulation. *J. Phys. Cond. Mat.* **2002**, *14*, 2745–2779.
(23) Kohn, W.; Sham, L. J. Self-Consistent Equations Including Exchange and Correlation Effects. *Phys. Rev.* **1965**, *140*, 1133–1138.
(24) Jung, J. H.; Park, C. H.; Ihm, J. A Rigorous Method of Calculating Exfoliation Energies from First Principles. *Nano Lett.* **2018**, *18*, 2759–2765.
(25) Negishi, H.; Negishi, S.; Kuroiwa, Y.; Sato, N.; Aoyagi, S. Anisotropic Thermal Expansion of Layered MoO3 Crystals. *Phys. Rev. B* **2004**, *69*, 1–3.
(26) Hautier, G.; Ong, S. P.; Jain, A.; Moore, C. J.; Ceder, G. Accuracy of Density Functional Theory in Predicting Formation Energies of Ternary Oxides from Binary Oxides and Its Implication on Phase Stability. *Phys. Rev. B* **2012**, *85*, 155208.
(27) Carcia, P. F.; McCarron, E. M. Synthesis and Properties of Thin Film Polymorphs of Molybdenum Trioxide. *Thin Solid Films* **1987**, *155*, 53–63.
(28) Kumar, A.; Ahluwalia, P. K. A First Principle Comparative Study of Electronic and Optical Properties of 1H-MoS_2 and 2H-MoS_2. *Mat. Chem. Phys.* **2012**, *135*, 755–761.
(29) Huang, Y. L.; Chen, Y.; Zhang, W.; Quek, S. Y.; Chen, C. H.; Li, L. J.; Hsu, W. T.; Chang, W. H.; Zheng, Y. J.; Chen, W.; et al. Bandgap Tunability at Single-Layer Molybdenum Disulphide Grain Boundaries. *Nat. Commun.* **2015**, *6*, 6298.
(30) Howell, S. L.; Jariwala, D.; Wu, C. C.; Chen, K. S.; Sangwan, V. K.; Kang, J.; Marks, T. J.; Hersam, M. C.; Lauhon, L. J. Investigation of Band-Offsets at Monolayer-Multilayer MoS_2 Junctions by Scanning Photocurrent Microscopy. *Nano Lett.* **2015**, *15*, 2278–2284.
(31) Coehoorn, R.; Haas, C.; Dijkstra, J.; Flipse, C. J. F.; De Groot, R. A.; Wold, A. Electronic Structure of $MoSe_2$, MoS_2, and WSe_2. I. Band-Structure Calculations and Photoelectron Spectroscopy. *Phys. Rev. B* **1987**, *35*, 6195–6202.
(32) O'Hare, P. A. G.; Lewis, B. M.; Parkinson, B. A. Standard Molar Enthalpy of Formation by Fluorine-Combustion Calorimetry of Tungsten Diselenide (WSe_2). Thermodynamics of the High-Temperature Vaporization of WSe_2. Revised Value of the Standard Molar Enthalpy of Formation of Molybdenite (MoS_2). *J. Chem. Thermodyn.* **1988**, *20*, 681–691.
(33) Kam, K. K.; Parkinson, B. A. Detailed Photocurrent Spectroscopy of the Semiconducting Group VI Transition Metal Dichalcogenides. *J. Phys. Chem.* **1982**, *86*, 463–467.